STATISTICAL ASPECTS OF COEXISTING FATIGUE FAILURE MECHANISMS IN OFHC COPPER

by

P. J. Haagensen

Manuscript recieved November 1966

JUNE 1967 UTIAS TECHNICAL NOTE NO. 112

ACKNOWLEDGEMENT

The author is indebted to Dr. G. N. Patterson, Director of the Institute for Aerospace Studies, for providing the opportunity to work on this project, and to Dr. G. K. Korbacher for his interest in the progress of the work and the supervision of the project.

This research project was sponsored jointly by the National Aeronautics and Space Administration and the National Research Council of Canada, Dr. G. K. Korbacher being the principle investigator.

The author also wishes to thank Dr. S. R. Swanson, Senior Research Engineer, De Havilland Aircraft of Canada Ltd., for his advice and co-operation throughout the period of the project.

Thanks are also due to Mr. F. Cicci, De Havilland Aircraft of Canada Ltd., Messrs. J. Burt and J. L. Bradbury of the Technical Staff of the Institute for Aerospace Studies for their valuable assistance, and to Dr. P. C. Hughes for his assistance in the development of the computer programs.

SUMMARY

This note presents the results of a series of axial-load, constant amplitude fatigue tests at zero mean stress on oxygen-free, high-conductivity (OFHC) copper specimens. A total of 631 specimens were tested at four stress levels near the lower "knee" of the S-N curve.

The log-normal (Gaussian) and the Weibull (Extreme Value) distribution functions were fitted to the complete sample of test endurance data at each of the four stress levels. A combination of two log-normal distribution functions and a combination of a log-normal and a Weibull distribution function were also applied since at all stress levels a two mode single, or bimodal distribution representation appeared feasible.

The main results of this study are:

1. At all four stress levels tested, the existence of two modes in the endurance distributions was indicated by (a) the apparent bimodality in the endurance histograms, (b) the significantly different values of the standard deviations of the low-endurance and high endurance components respectively, and their consistency with stress level, and (c) by the consistent variations in the parameters of the low-endurance log-normal component distributions as determined by the truncation method.

2. The overall standard deviation was found to be largest for the highest stress level.

3. The single Weibull distribution function gave the best fit not only for the endurances at each stress level but also for the high-endurance components at all stress levels.

4. The better estimates for the parameters of the Weibull distribution functions were obtained by the upper vertical moment rather than the classical moment method.

TABLE OF CONTENTS

NOTATION

b	Weibull shape parameter
E	Young's modulus
f(N)	Weibull frequency distribution function
F(N)	Weibull cumulative probability function
$F_1(N)$	Extreme value cumulative probability function
I	Moment of intertia of a cross section in bending. For a circular cross section, I is given by $D^4/64$; for a square cross section of width B, I is given by $B^4/12$
ksi	Thousands of pounds per square inch
LTF	Long Term Fatigue - designating the high-endurance component in a bimodal distribution
l_a	Length of the free (ungripped) part of the alignment specimen
l_f	Length of the parallel test section of the fatigue specimen
$\log_{10}$	Common logarithm (base 10)
ln	Natural logarithm
M	Bending moment
M_L	Slope of the regression line
M'	Bending moment at the strain gauges on the alignment specimen
M_a	Bending moment due to angular displacement,
M_t	Bending moment due to translational displacement,
n	Total number of observations in the sample of a population
n_{tr}	Number of observations, the endurance values of which are known in a truncated sample
N	The endurance of a specimen in cycles
N_i	The ith endurance when the N values have been arranged in ascending sequence

N_o — The minimum life parameter. N_o is defined by the probability $F(N \leq N_o) = 0$

$\overline{N}^m$ — (Mean of N)^m = $\left(\frac{1}{n}\sum_{i=1}^{n} N_i\right)^m$

$\overline{N^m}$ — Mean of(N^m) = $\frac{1}{n}\sum_{i=1}^{n} N_i^{\,m}$

psi — Pounds per square inch

P_i — Plotting position

p(x) — Normal frequency distribution function, given by

$$p(x) = \frac{1}{\sigma\sqrt{2\pi}} \exp.\left[-\frac{(x-\mu)^2}{2\sigma^2}\right]$$

P(x) — Normal cumulative distribution function given by

$$P(x) = \int_{-\infty}^{x} p(x)\,dx$$

r — Correlation coefficient

STF — Short Term Fatigue - designating the low-endurance component in a bimodal distribution

s^2 — Estimate of the variance σ^2 obtained from a sample containing n observations. It is given by

$$s^2 = \frac{1}{n-1}\sum_{i=1}^{n}\left(x_i - \bar{x}\right)^2$$

s — Sample standard deviation. s is an estimate of the population standard deviation σ

s_{xy} — Covariance of x and y, given by

$$S_{xy} = \frac{1}{n-1}\sum_{i=1}^{n}(x_i - \bar{x})(y_i - \bar{y})$$

S_a — Nominal stress amplitude in ksi

t_α — Value of the t variate which will bracket α of the probability

V — Characteristic life parameter in the Weibull distribution; V is defined by $F(V) = 1/e$

x — $\text{Log}_{10}(N)$

x_i — The ith of the ranked values of x

$\bar{x}$ — Mean of x_i, given by $\bar{x} = \frac{1}{n}\sum_{i=1}^{n} x_i$

y	Distance in inches from the specimen neutral axis to the point at which the bending stress σ_B is being calculated
z	Standardized point of truncation
Z	Section modulus = $I_{/y}$
α	Probability that an interval will contain the true mean;
α	Angular displacement of one(gripped) end of the specimen with respect to the other
$\sqrt{\beta_1}$	Skewness parameter of the Weibull distribution function (Classical moment method)
δ	Translational displacement of one (gripped) end of the specimen with respect to the other
ϵ	Strain in micro inches (min.) per inch
$\Gamma(p)$	Complete gamma function, given by $\Gamma(p) = \int_0^\infty e^{-y} y^{p-1} dy$
μ	Population mean
μ_3	Third central moment about the mean
σ_B	Bending stress
σ^2	Variance of a population
σ	Population standard deviation

I. INTRODUCTION

The large scatter observed in fatigue endurances of nominally identical specimens subjected to nominally identical load cycles has lead to the recognition of fatigue failure as a statistical phenomenon. Some of the scatter can be attributed to random variations and errors in the applied loads, to inherent inaccuracies (e. g. alignment) in the fatigue machine, and to non-uniform test conditions (environmental changes) and test procedures. Variations in specimen properties, surface conditions, dimensions and geometry due to manufacturing tolerances and processes, also contribute to this type of scatter. Furthermore, a number of material properties affect the endurance scatter. For example, material fabrication history (heat treatment and cold work prior to testing); grain size and orientation; submicroscopic defects such as inclusions, vacancies, lattice stacking faults, dislocation density, etc.

Because of this scatter, constant amplitude fatigue results can be effectively presented only by a relation between the stress of amplitude S, the endurance N, and the probability P that any specimen subjected to a given number of load cycles of the stress amplitude S will fail at or before N cycles are reached. For a structural element subjected to fatigue loading it is (for practical and economic reasons) not feasible to design for zero probability of failure, and usually a very small but finite risk of failure must be assumed. The accuracy of the probability function on which this risk is based, is thus of great importance for the designer.

In the analysis of constant stress amplitude fatigue test results, several distribution functions have proven useful in representing the test endurance data. Perhaps the best known is the log-normal or Gaussian which assumes the log of the number of cycles to failure to be normally distributed. This distribution, and others such as the extreme value distribution, fit the data well, especially near the mode of the distribution.

Usually the best fit of constant amplitude test data to any particular type of distribution is found at high stress levels. At the "knee" of the S-N curve, the scatter seems to be larger and extrapolation into probability ranges not covered by test data becomes quite dubious. In this stress range, also a discontinuity in the S-N curve has been reported. (Refs. 1, 2 and 3).

Certain observations of a large scatter and discontinuity at the knee of the S-N curve have been interpreted by Swanson (Refs. 4 and 5) and Cicci (Ref. 6) as being the result of a blending of two endurance distributions caused by two coexisting failure mechanisms. One is predominantly causing failure above the knee, the other one below it. The knee itself is the transition region characterized by the gradual decay in probability of occurrence of the one failure mechanism and the growth of the other. Thus, according to this concept, at any stress level within the transition region a compound failure probability exists due to the component failure

probabilities from the two mechanisms.

Also from a metallographic point of view, there are reasons for considering the knee as a transition region. W. A. Wood (Ref. 7) has on the basis of observed fatigue-induced microstructural differences divided the generalized S-N curve into three strain amplitude ranges, H, F and S. In the H range, endurances increase only slightly with decreasing stress, in the F or intermediate range, a small reduction in stress amplitude gives a very large increase in endurance, and in the S or pseudo-safe, low stress range, the endurances approach infinity. Thus, the knee can be considered as a transition region where each stress level is characterized by the amount of H, F and S-type fatigue damage present in the microstructure.

The present investigation was undertaken to check the existance of bimodal endurance distributions on a sound statistical basis. Instead of alloys, for which some evidence exists (Ref. 5), OFHC copper was chosen as the test material. At least 150 specimens were to be fatigue tested at each of four stress levels around the lower knee of the S-N curve under axial, constant amplitude loading. OFHC copper was chosen because of its simple and clean microstructure which is well suited for a subsequent metallographic examination of the failed specimens. (see Ref. 8)

II MATERIAL, APPARATUS AND TEST PROCEDURE

2.1 Specimen material:

The material used for this series of tests was certified OFHC copper of 99.95% + purity. The copper was supplied by Anaconda Co. (Canada) Ltd. in the half-hard cold drawn state in the form of 3/4" dia., 12 ft. long rods.

The rough-machined specimens were annealed for two hours at 1050°F in a vacuum of 0.025 mm Hg in batches of 200. After machining they were fine machined to final dimensions (Fig. 2).

To check the uniformity of the heat treatment and to obtain samples of the mechanical properties, seven control specimens were picked out at random from each batch. These specimens were tested in an Instron tensile testing machine and their mechanical properties are listed in Table I. The specimens were found to be extremely soft. This resulted in some difficulties in the tensile tests and may account for the comparatively large scatter in the test results.

While the annealing process provided complete stress relaxation of the specimens, the annealing temperature and time were insufficient to bring about a complete recrystallization. Figure 1 shows a micrograph of the core of an untested specimen. The grain structure is characterized by a large variation in grain size and the presence of a number of partly

recrystallized grains.

The final machining caused the formation of a work-hardened layer at the surface. The depth of this layer, about 0.01 inch, was somewhat larger than expected.

Because of the large number of specimens involved the annealing and machining of the specimens had to be done outside the University and the conditions under which these processes were performed could therefore not be controlled as carefully as desirable.

2.2 Specimen Configuration and Preparation:

The shape and dimensions of the fatigue specimens are given in Fig. 2. To avoid stress concentration at the ends of the parallel test section the curvature at the fillets as shown was adopted. Photoelastic strain analysis (Ref. 9) has shown that this curvature practically eliminates sharp stress gradients.

Due to warping of the specimens during annealing the machining was done in two stages. First the specimens were rough machined leaving all diameters 0.025 in. oversize. A hole was drilled and tapped in one end so that the specimens could be annealed in the hanging position. After annealing the final machining was done by taking passes of 0.0025 in. depth at a feed of only 0.002 in. per revolution.

The specimen dimensions were measured prior to testing using an optical comparator. The test section diameter was measured at three locations, at each end and at midlength. The eccentricity was measured at the same locations. It was found that the diameters at the fillets were consistently smaller by about 0.001 in. than those measured at midlength. This was most likely due to a slight undercut on the template used in the machining. The loads used in testing were always calculated using the smallest cross-section diameter. Specimens having eccentricities exceeding 1/1000 in. (measured at midlength) were rejected.

2.3 The Fatigue Machine:

The machine used for this investigation was of a patented type (Ref. 10), the driving force being supplied by an electromagnetic shaker of 25 lbs. maximum load capacity. A schematic diagram of the machine is shown in Fig. 3 and a photograph of the machine and its instrumentation is shown in Fig. 4.

The dynamic system consists of the shaker, (see Fig. 3 and 5b), a lever hinged at one end by crossed flat steel springs, the load-transmitting vertical springs which also serve as load dynamometor (the springs are strain-gauged) and the lower (moving) gripping head. The lower head is mounted on parallel springs which allow movement in the

vertical direction only, without rotation of the head. The upper gripping head is rigidly connected to the machine structure. It was made adjustable in the vertical direction in order to turn the lever to a reference position after the specimen was clamped in the grips.

The gripping arrangement is also shown in Fig. 5a. The grips are standard "rubber-flex" collets with wedge-shaped hardened steel plates which have been hook-serrated to give firm gripping action. To insert a specimen the sliding block (see Fig. 5a) is pushed back and the specimen is lowered into the collet. The collet compression disk is then tightened until the specimen is firmly gripped. Returning the sliding block, the back-up pin is tightened against the end of the specimen. By alternately tightening the collet compression disk and the back-up pin, the specimen is firmly clamped and able to withstand both tension and compression axial dynamic loading, without slipping in the grips. The gripping heads, which are free to move during the gripping procedure, are then moved to and locked in their reference position. This gripping arrangement has proved very satisfactory. In none of the tests was there any evidence of slipping of the specimen in the grips.

The input signal to the shaker was an amplified sine-wave from an audio oscillator. The resonance frequency of the specimen-shaker-lever system was approximately 80 cps. The maximum alternating load amplitude obtained with a copper specimen was about 1000 lbs. With added weights (24 lbs) attached to the lever, the maximum load could be increased to about 1100 lbs., however, the resonant frequency was then reduced to about 57 cps. The weights had to be used for the highest stress level (16.5 ksi) used in this program. The reduction in frequency is not considered to have a significant effect on the fatigue properties, as concluded by Stephenson in Ref. 11.

The signal from the dynamometer strain gauges was amplified by a bridge pre-amplifier and measured by an electronic voltmeter. The dynamic component of the signal was used to drive a photo-electric controller with two cut-out points. The high point was used to switch on a warning light when the load dropped below a preset value. The low cut-out point de-energized the main power supply relay (for the shaker amplifier and certain instruments) and thus served as a shut-off device. The total number of cycles to failure was recorded by an electronic counter operating on the oscillator signal. The testing time was measured by an ordinary electric wall clock in the controller circuit. This provided a rough check on the counter since the number of cycles to failure could be calculated, if necessary, from the total testing time and the frequency.

2.4 Machine Calibration:

A special calibration specimen was made up from 7075-T6 aluminum alloy. The middle portion of this specimen was square-sided with a 0.45 x 0.45 in. cross-section while the cylindrical gripping ends were

of the same diameter as the gripping ends of the fatigue specimens. Two opposite faces were strain gauged, the gauges being wired in a Wheatstone bridge to measure longitudinal strains only.

The calibration specimen was first calibrated in a Tinius Olsen tensile testing machine using a strain indicator. Then the specimen was placed in the fatigue machine and the load dynamometer calibrated statically, using the mean stress spring to apply load to the specimen.

In the dynamic load calibration a load monitoring system, consisting of an oscilloscope, a strain indicator and a bridge pre-amplifier was used. First the oscilloscope was calibrated statically using the bridge output, the load being set up with the calibration specimen and the strain indicator. Starting the machine and adjusting the load, the dynamic signal was made equal in magnitude to the previous static signal. Disconnecting the oscilloscope with the machine running, the pre-amplifier-voltmeter circuit was connected to the dynamometer and the load calibration for the voltmeter was obtained.

2.5 Machine Accuracy :

Since this investigation was aimed at determining the endurance distributions as a material property, great care was taken during assembly and calibration of the machine to avoid random errors resulting from inaccuracies in the machine and load-measuring devices.

An inherent source of errors in axial-load fatigue machines is the gripping arrangement. Slightly inaccurate alignment of the grips will introduce large errors. For commercial machines, errors ranging from 2 up to 20 per cent have been measured (Ref. 12).

For the final alignment of the grips, a strain-gauged steel specimen with a square cross-section between the grips was made. The strain gauges were mounted on all four faces, and those on opposite faces were wired in pairs in a Wheatstone bridge to measure bending strains only. One set consisting of two pairs of gauges was mounted vertically at each end of the free-length portion of the specimen thus making it possible to take readings of the bending strain at two points in each of two vertical planes at right angles to each other. With the machine's lower gripping head completely loose, the specimen was gripped at both ends and the lower head was adjusted to minimize the bending strains.

It was found, however, that in spite of alignment to better than 1/1000 in., strains could not be completely eliminated. An analysis of the effect of residual misalignment on the stress in the test piece was carried out (Appendix E) using the residual strain readings. While this analysis shows that the resulting stresses in the fatigue specimen are still appreciable, it is emphasized that this type of error is constant for all specimens tested at the same stress level and should therefore not

affect their endurance distribution.

A complete analysis of the possible errors in dynamic load is very complex and was not carried out in detail. However, on the basis of an assessment of the accuracies of the individual instruments involved, it is estimated that the maximum error in dynamic load is of the order of about 1.5%. This is confirmed qualitatively by the data obtained from the tests at the two lowest stress levels, 13.0 ksi and 12.7 ksi. Although the spacing of these stress levels is only about 2.4% of the stress amplitude, there is a significant difference in the mean endurance.

2.6 Test Procedure:

Particular care was taken in the operation of the machine to keep experimental errors to a minimum. After insertion in the machine a mark was placed on the specimen near the lower grip to facilitate later a crack position correlation with the position of the specimen in the machine.

In nearly all tests, the crack initiated at the same location on the specimen, namely at the front of the lower fillet. Two factors accounted for this. First, it was found that the slight undercut in the test section diameter was always located at this lower fillet. Secondly, the calculations carried out in Appendix E show that the largest bending strain due to misalignment of the grips was present at the front of the lower fillet. The other maximum value of the bending strain occurred at the back of the top fillet and this was where the crack started on those few specimens that did not fail at the lower fillet.

Since uniformity of the specimens within a group tested at the same stress level was considered of greater importance than uniformity between specimens tested at different stress levels, it was decided to use at each stress level specimens from one heat treatment batch only.

Prior to each test the bridge pre-amplifier and the electronic voltmeter were zero-checked and calibrated.

During the first 3 minutes of each test it was found necessary to reduce the power input to the machine continuously because of extensive work-hardening in the specimen. During this period of 10,000 - 12,000 cycles, the resonant frequency also changed slightly. After the starting period the load had to be re-adjusted (slightly upward) at intervals of approx. 15 min. for the higher stress levels while at the lower stress levels, similar load adjustments were necessary only every 2-3 hours.

The amount of heat produced in the fatigue specimens due to energy dissipation at the higher stress levels was quite noticeable. To obtain some idea of the temperature increase in the specimen, a thermocouple was attached to the test section of some of the specimens and the

temperature recorded continuously throughout the test. A description of these measurements is found in Appendix F.

2.7 Environmental Conditions:

All tests were done at room temperature and uncontrolled room humidity. Since the laboratory in which the fatigue machine was located is surrounded by other rooms and has no direct openings to the outside, and since the bulk of the testing was done at a time of the year when indoor heating was used, relatively small variations in humidity and temperature were recorded. Fig. 6 shows a typical plot of temperature and humidity versus log (cycles to failure). While no correlation is apparent between temperature and endurances, there is a slight correlation favouring low endurances at high values of relative humidity.

III. THE DISTRIBUTION FUNCTIONS

In the interpretation of fatigue data the endurances are usually assumed to be distributed in such a manner as to form a single distribution. The assumption of more than one failure mechanism operating at any one stress level and causing the endurances to group around characteristic mean values for each mechanism, leads to the concept of a heterogeneous endurance population, i.e. an endurance distribution containing two or more modes.

The test endurances are plotted in histograms (Fig. 7) using a class length of 0.01 log N. All plots, except the one for the lowest stress level, show a dip or "valley" to the left of the peak of the distribution. Assuming that the secondary peak to the left is significant, it could be interpreted as evidence for a two-mode or bimodal distribution (schematically indicated by dashed lines in Fig. 7).

Two types of distribution functions were considered for best fit to the overall test endurance distributions, namely the log-normal or Gaussian, and the Weibull (Extreme Value). Combinations of (a) two log-normal distributions and (b) a log-normal and a Weibull distribution function were also applied at all stress levels.

Appendix A, B and C give the theoretical background for the calculation of the parameters for the single (undivided) and truncated distribution functions of the two types used.

IV. ANALYSIS OF RESULTS

4.1 The Control Tensile Specimens:

The arithmetic mean and standard deviation of the various properties were calculated by the standard formulae. The results are listed in Table I.

The true mean μ will lie between the limits

$$\bar{x} \pm t_{\alpha} \, s \, / \sqrt{n}$$

where t_{α} depends on the number of values measured, n, and the degree of confidence required, α . Choosing α = 95%, i.e. the probability that the interval $\bar{x} \pm t_{\alpha} \, s \, / \sqrt{n}$ contains μ is 95% results in $t_{\alpha} = 2.04$ (Ref. 21). The 95% confidence limits are given for the more important properties in Table I.

4.2 Single Log-Normal Distribution:

Considering the test endurance distribution to be a single log-normal distribution, the parameters x and s were calculated, using the standard formulae given in the Notation. These parameters are listed in Table III. The endurance data for the four test stress levels are plotted as single distributions on log-normal probability paper in Fig. 8. Using the method of least squares a linear regression was carried out on the relation between ranked endurances and probability. The solid lines on the plots are the regression lines. The correlation coefficient is given in each case on the plots.

The slopes of the regression lines and the standard deviation in Table III show that the variance of the distribution for the lowest stress level (12.7 ksi) is less than that at the highest stress level, while the variances for the two other stress levels have intermediate values. This is rather unusual; instead of increasing scatter with decreasing stress as one conventionally expects, at least for alloys, the scatter of the endurances in the present results varies in a rather unconventional manner from one stress level to another.

The probability plot for the 16.5 ksi stress level shows that the endurances fit very closely to the single distribution regression line. The random manner with which the points are scattered about this line seems to suggest that the sample is drawn from a single normal population.

The test data for the intermediate stress levels (14.0 and 13.0 ksi) do not fit as well to a straight line and there is an orderly trend in their deviation from the regression line which, however, can also be detected at the 16.5 ksi stress level. Below a probability of failure of approximately 30%, the curves for all three levels are scattered about a line (dashed line) with a lower slope than the regression line. Above 30% probability there is a transition region up to about 40%, above which the points seem to fit closely to another straight line (dashed in Fig. 8.). This line is steeper than the regression line. Both dashed lines were fitted visually. The interpretation of the two dashed lines implies that there could be two components in the endurance distribution for each of the three stress levels, the parts below 30% probability of failure having a smaller variance than those above, demonstrated by the difference in slope. The heterogeneous

nature of the three samples is also demonstrated by the histogram plots of the fatigue endurances in Fig. 7, which exhibit a double "hump" for the three highest stress levels and a degenerate form of bimodality at the 12.7 ksi level.

The probability plot for the 12.7 ksi stress level (Fig. 8) shows that the endurances fit the regression line rather poorly. But note that they follow a smooth curve better than the two dashed lines. This may be taken as an indication that the lower bound of the distribution is non-zero and that a three-parameter distribution function is required, (Ref. 12), to represent the test endurances best. This is confirmed by the cumulative frequency plot for this stress level (Fig. 9), where the data fit the single log-normal distribution curve poorly, except in the high-endurance part. (In Fig. 9 the curves for the two Weibull distribution functions are drawn for comparison. It should be noted, however, that these distribution functions were calculated for the distribution of N (cycles), not log (N), which is the abscissa in Fig. 9. The correlation coefficients given elsewhere for these distribution functions do therefore not apply to Fig. 9).

4.3 Single Weibull (Extreme Value) Distributions:

4.3.1 Classical Moment Method-

Following the procedure in Appendix B, the estimate of the skewness parameter was calculated from Eq. B.8 using the University of Toronto IBM 7090/7094-11 computer. Using Table I in ref. 13 the parameters b, A(b), and B(b) were found and N_o and V were calculated from Eqs. B.11 and B.10 respectively. With these values a regression analysis was carried out and the data plotted on extreme value probability paper, using the plotting position of Eq. D.8. These plots are shown in Fig. 10, with the values of the parameters, N_o, and the correlation coefficients, r, given in each case. All the Weibull parameters and correlation coefficients are listed in Table IV.

The way the experimental points in Fig. 10 are scattered about the regression lines shows that the estimates of the parameters are quite good. For instance, the effect of an incorrect estimate of N_o is to bend the curve away from the regression line at the tails of the distribution. The overall correlation coefficients are in all cases, except the lowest stress level (12.7 ksi), smaller than those for the log-normal representation, but the differences are very small.

4.3.2 Method of Upper Vertical Moments -

Using the procedure outlined in Appendix C the parameters b, N_o and V were calculated from Eqs. C.11, C.12 and C.19, respectively, using Eqs. C.14 and C.15 to estimate the upper vertical moments. The values of these parameters differ somewhat from those obtained by the classical moment method, but the differences are small considering the large

influence which small numerical variations in the $\bar{x}_r$ values have on the parameters. The difference in the shape of the frequency distribution functions for the upper vertical moment method as compared with those obtained by the classical moment method is also small, as demonstrated in Fig. 12.

The parameters N_o, and the correlation coefficients, obtained by a regression analysis identical to that in the preceding section, are listed in Table V. It is seen that the estimates of the parameters of the Weibull distribution functions by the method of upper vertical moments give correlation coefficients which in all cases are higher than those for the log-normal distribution, and also higher than those calculated by the classical moment method. This is further illustrated in Fig. 11 by the close fit of the endurances to the regression lines.

4.4 Two Log-Normal Distributions:

In representing the endurance data at one stress level as a combination of two distribution functions, the problem of dissection of the endurance distribution arises since the components obviously are overlapping (see Fig. 7). The method used here is to calculate the two sets of parameters, using only the tail ends of the combined distributions, i.e. to truncate the data so that only the observations above and below the overlap region are used for the determination of the parameters. Assuming the tail ends to be parts of normal distributions, one should find that after some initial variation in the estimated parameters for small samples, the parameters should approach stable values as the truncation point is approaching the centre of the undivided distribution.

Using the procedure outlined in Appendix A, the parameters $\bar{x}$ and s were calculated taking as the truncation point x_{tr}, the arithmetic mean of the logarithms of two adjacent endurances of the last (or first, depending on which tail end is considered) endurance in front (or behind) and the first (or last) endurance in the overlapping region. Using the IBM computer it was possible to calculate $\bar{x}$ and s for a wide choice of truncation points, in fact for nearly all endurances with the exception of the extreme tail ends. The calculated parameters are plotted versus the number of specimens in the truncated sample, n_{tr}, for the low-endurance part in Fig. 14. For comparison the values of $\bar{x}$ and s calculated for the single log-normal distributions representing all endurances at each stress level are indicated on the graphs.

The large, apparently random variations in the parameters for the lowest stress level, 12.7 ksi, show that the sample is very irregular and the truncated log-normal distribution in this case is very unreliable for the estimation of the parameters. The results for the three highest stress levels, however, show a trend. After initially large variations of $\bar{x}$ and s for small values of n_{tr}, a region is reached in which there is an abrupt drop in the values of the parameters, corresponding to the dip in the histo-

gram plots in Fig. 7 and to the jog in the probability curves in Fig. 8. After this drop the parameters increase in a more or less uniform manner to reach the values of the parameters for the single log-normal distributions as upper limits (see Fig. 14).

Assuming this abrupt drop to indicate the extent of the predominance of the STF component mode the corresponding total number of specimens in the STF mode were estimated by taking twice the number of specimens the endurances of which were lower than that for the mean, $\bar{x}$, specified by the drop. These estimates of the STF parameters and the number of specimens in each STF mode are given in Table VI. In the histograms the STF (shaded) component represents approximately the value of n_{tr} corresponding to the chosen values of $\bar{x}$ and s, except for the 12.7 ksi case in which the STF component was estimated from the histogram. The number of specimens in the STF component (shaded part in the histograms) is plotted for the top three stress levels on log-normal probability paper (Fig. 16) taking the total cumulative probability for each STF mode equal to unity. The plots show that the low-endurance (STF) component is well represented by a log-normal distribution.

Although the histograms show that the STF components in some cases are slanted to the right (toward the high-endurance part), it was not attempted to represent the STF components also by a Weibull distribution since the skewness to the right implies an upper bound, a "maximum life" rather than a minimum life parameter, thus contradicting the underlying assumptions for the extreme value distributions (the "weakest link" concept). The apparent skewness could be explained by the fact that the component distributions are strongly overlapping.

The parameters obtained by considering the high-endurance tail end truncated (i.e. known) are plotted in Fig. 15. Only the two intermediate stress levels are considered. In the case of the 14.0 ksi stress level, there is an abrupt drop similar to that observed in Fig. 14b for the low-endurance case, when the sample comprises about 90 specimens. This drop corresponds to the discussed dip in the histogram of Fig. 7c, but the value of $\bar{x}$ in this region is so low that it gives the estimated number of specimens in the LTF distribution at about 170, a number which is larger than the number of specimens tested at this stress level. At the 13.0 ksi level the parameters vary in such a manner that a clear indication of the LTF range extent cannot be obtained. The plots for the highest and lowest stress levels showed a similar behaviour. These results, and the obvious skewness to the left of the LTF distribution which the histograms show, suggest that a representation of the LTF component by a log-normal distribution would give a very poor fit. The endurance data for the high-endurance components at all stress levels were therefore not plotted on log-normal probability paper and no regression analysis was carried out.

4.5 Combined Log-Normal and Weibull Distributions:

Using the same log-normal distribution functions as calculated in the preceeding section to represent the STF components, the Weibull distribution functions for the high-endurance components were calculated using the upper vertical moment method. The parameters were computed for a range of truncation points and regression was carried out in each case. The degree of truncation which gave the highest correlation coefficient was chosen and the resulting distributions are plotted on extreme value probability paper in Fig. 17. The values of the N_o parameters is given on the graphs together with the correlation coefficients. It is seen that the fit is not as good as in the single Weibull (upper vertical moment method) presentation. (Fig. 11).

The standard deviation for both N and log N were calculated for the LTF component using the formula given in the Notation. The endurances used were all those greater than N_o. The values of the standard deviations and the parameters of the LTF Weibull components are listed in Table VII.

A S-N curve showing the endurance scatter ranges, the means of the (log-normal) STF and the (Weibull) LTF modes as well as the means of the Weibull single distributions is shown in Fig. 13(a).

The standard deviations for the STF and LTF modes and for the single distributions are plotted in Fig. 13(b). It is seen that the standard deviations for the STF and LTF modes are consistently lower at all stress levels and are in all cases highest at the highest stress level. The factor of two in the standard deviations, by which the STF and LTF modes are separated is the most convincing evidence that the endurances represent a single distribution with two modes, or a bimodal distribution.

V. CONCLUDING REMARKS

The axial-load fatigue endurance distributions of annealed OFHC copper specimens with a cold-worked surface layer, tested at four stress levels under constant-amplitude tension-compression, form the basis for the following observations:

1. Evidence for the existance of two modes in the endurance distributions is indicated by three features of these distributions:

   (a) The apparent bimodality in the endurance histograms.
   (b) The significantly and consistently different values at all stress levels for the standard deviations of the STF and LTF modes respectively.
   (c) The consistent variations in the STF parameters obtained by the maximum likelihood truncation method.

Further refinements of the analysis leading to the estimation of the parameters of the underlying component distributions (e. g. the method of maximum likelihood being applied to the data where the underlying distribution is assumed to be composed of (STF) log-normal component and (LTF) Weibull component are possible, but would not remove the ambiguity in the identification of the endurances in the overlap region.

Earlier observations in the literature of the bimodal phenomenon with two well-separated component distributions may possibly be explained by the fact that the materials involved were alloys, while in the present investigation a pure metal was tested. This difference is worthy of further investigation.

2. The overall standard deviation was largest for the highest stress level, decreasing with decreasing stress amplitude.

3. Using the correlation coefficient as criterion for the "goodness of fit" of the distribution functions to the test data in addition to a visual comparison of the probability plots, the following conclusion can be drawn:

(a) Single Weibull (Extreme Value) distribution functions, with the parameters calculated by the upper vertical moment method in all cases fitted the test data better than log-normal functions.
(b) Log-normal distribution functions, due to the apparent symmetry of the STF modes of the test data gave the expected good fit, but the
(c) LTF modes could be represented best by Weibull distribution functions.
(d) The best estimates of the parameters for the Weibull distribution functions were obtained by the method of upper vertical moments.

REFERENCES

1. Williams, T. R. G. — The Extrusion Characteristics and Mechanical Properties of Aluminum Alloy L-65. A. A. S. U. Report No. 189, August 1961.

2. Lowcock, M. T. Williams, T. R. G. — Effect of Random Loading on the Fatigue Life of Aluminum Alloy L-73. A. A. S. U. Report No. 225, July 1962.

3. Shabalin, V. I. — Discontinuity in the Fatigue Curve for Duralumin. Metal Industry, January 1959.

4. Swanson, S. R. — Systematic Axial Load Fatigue Tests Using Unnotched Aluminum Alloy 2024-T4 Extruded Bar Specimens. U. T. I. A. Techn. Note. No. 35, May, 1960.

5. Swanson, S. R. — Practical Fatigue Loadings for Aeronautical Structures. Fourth Congress, International Council of the Aeronautical Sciences, Paris, Spartan Press. August, 1964.

6. Cicci, F. — An Investigation of the Statistical Distribution of Constant Amplitude Fatigue Endurance for a Maraging Steel. U. T. I. A. S. Techn. Note No. 73, July, 1964.

7. Wood, W. A. — Experimental Approach to Basic Study of Fatigue. Institute for the Study of Fatigue and Reliability, Report No. 24, Columbia University, August, 1965.

8. Muggeridge, D. B. — An Attempt to Correlate Fatigue Endurance Distributions in OFHC Copper to Wood's H, F and S Ranges. U. T. I. A. S. Techn. Note No. 111, October, 1966.

9. Swanson, S. R. — An Improved Law of Cumulative Damage. College of Aeronautics, Report 148, Cranfield, England, August, 1961.

10. Swanson, S. R. — An Investigation of the Fatigue of Aluminum Alloy Due to Random Loading. U. T. I. A. Report No. 84, February, 1963.

11. Stephenson, N. — A Review of the Literature on the Effect of Frequency on the Fatigue Properties of Metals and Alloys. NGTE M-320, June, 1958.

12. Weibull, W. — Fatigue Testing and Analysis of Results. Pergamon Press, 1961.

13. Freudenthal, A. M. Gumbel, E. J. — Minimum Life in Fatigue. Journal of the American Statistical Association, Volume 49, November, 1954.

14. Weibull, W. — A Statistical Representation of Fatigue Failure in Solids, Trans. Royal Institute of Technology, No. 27, Stockholm, 1949.

15. Weibull, W. — The Phenomenon of Rupture in Solids, Handlingar Ingeniörs Vetenskap Akademien, No. 153, Stockholm, 1939.

16. Weibull, W. — New Methods for Computing Parameters of Complete or Truncated Distributions, FFA Report 58, Aeronautical Research Inst. of Sweden, February, 1955.

17. Pearson, K. — Tables of the Incomplete Gamma-Function, Cambridge, 1951.

18. Hald, A. — Maximum Likelihood Estimation of the Parameters of a Normal Distribution which is Truncated at a Known Point. Skandinavisk Actuarietidskrift, 1949.

19. Hald, A. — Statistical Theory with Engineering Applications. John Wiley & Sons.

20. Blom, G. — Statistical Estimates and Transformed Beta-Variables. Stockholm, 1958.

21. — Statistical Processes Based on the Gaussian Distribution.

21.	continued	Data Sheets A. 00. 05, Royal Soc. of Aeronautics, September, 1959.
22.	Fraser, D. A. S.	Statistics: An Introduction. John Wiley & Sons, 1958.
23.	Niles, A. S. Newell, J. S.	Airplane Structures, Vol. 1, John Wiley & Sons, 1954.
24.	Clarebrough, L. M. Hargreaves, M. E. Head, A. K. West, G. W.	Energy Stored During Fatigue of Copper, Journal of Metals, January, 1955.
25.	Wadsworth, N. J.	Energy Dissipation During Fatigue Tests. (Article), Dislocations and Mechanical Properties of Crystals. John Wiley & Sons, 1956.

TABLE I

CONTROL TENSILE SPECIMEN DATA

Nominal Stress Amplitude S_a (ksi)	Specimen Number, * Designates Heat Treatment Batch	Diameter (Mean) (inches)	0.2% Proof Stress (psi)	Tensile Strength (psi)	$Ex10^{-6}$ (psi)	Elongation on 1 in. (%)	Area Reduction (%)	Diamond Pyramid Hardness of Unfatigued Material
12.7	D-1	.291	10,355	41,028	17.96	61.7	92.4	43.2
	D-2	.292	9,992	41,028	17.56	62.5	91.6	42.4
	D-3	.291	7,797	41,331	18.12	61.7	92.4	42.5
	D-4	.291	9,311	40,877	17.63	62.5	91.6	42.4
	D-5	.291	7,479	40,574	18.68	61.2	91.6	41.8
	D-6	.292	8,327	41,180	18.60	61.7	92.0	41.1
	D-7	.292	9,508	41,331	17.93	60.7	92.0	42.0
13.0	B-1	.292	10,053	40,877	16.93	59.3	91.8	44.6
	B-2	.291	8,175	40,574	17.43	60.0	92.0	42.2
	B-3	.291	9,190	40,423	16.86	59.3	92.0	42.4
	B-4	.291	8,281	40.726	17.85	59.4	91.8	43.9
	B-5	.292	8,705	40.271	17.27	59.7	92.6	42.4
	B-6	.292	9,493	40,877	17.20	60.0	91.8	43.1
	B-7	.291	9,356	40,726	17.10	59.1	92.6	44.6
14.0	A-1	.292	6,934	40,726	15.96	65.0	92.0	41.4
	A-2	.292	9,084	40,574	18.00	59.8	92.0	40.0
	A-3	.292	10,598	41,180	15.95	61.7	92.0	40.5
	A-4	.292	7,873	40.877	16.20	62.9	92.4	39.0
	A-5	.291	7,645	40,574	17,90	63.5	92.0	39.5
	A-6	.292	8,418	40,271	17.90	65.0	92.4	39.4
	A-7	.291	7,645	40,271	17.13	64.5	92.2	39.6
16.5	C-1	.292	10,885	40,877	16.60	61.7	92.6	44.4
	C-2	.292	9,417	40,877	17.40	60.4	92.0	43.9
	C-3	.292	9,538	41,180	16.70	62.1	92.6	44.7
	C-4	.291	10,219	40,574	16.60	61.8	92.4	43.9
	C-5	.292	9,614	40,574	16.85	60.1	91.8	41.6
	C-6	.292	8,705	40,877	16.75	61.6	91.8	41.7
	Mean ($\bar{x}$)		8,899	40,790	17.30	61.4	92.1	42.2
	Standard Deviation		1,042	306	0.73			
	95% Confidence Limits		8,490	40,670	17.01			
			9,308	40,910	17.59			

RANKED FATIGUE ENDURANCES

(CYCLES TO FAILURE) x 10^{-6}

Rank	12.7 ksi	13.0 ksi	14.0 ksi	16.5 ksi
1	0.7737	0.8215	0.3016	0.1224
2	0.8096	0.8426	0.3168	0.1245
3	0.8167	0.8427	0.3231	0.1274
4	0.9244	0.8476	0.3260	0.1306
5	0.9344	0.9172	0.3289	0.1308
6	0.9533	0.9210	0.3310	0.1322
7	0.9542	0.9220	0.3330	0.1347
8	0.9687	0.9225	0.3343	0.1366
9	0,9860	0.9328	0.3370	0.1385
10	1.0017	0.9474	0.3420	0.1399
11	1.0300	0.9481	0.3460	0.1409
12	1,0389	0.9674	0.3478	0.1413
13	1.0520	0.9746	0.3479	0.1434
14	1.0743	0.9771	0.3494	0.1436
15	1.0943	0.9779	0.3513	0.1457
16	1.1010	0.9786	0.3536	0.1464
17	1.1113	0.9830	0.3560	0.1484
18	1.1403	0.9884	0.3568	0.1490
19	1.1522	0.9891	0.3606	0.1493
20	1.1527	0.9936	0.3610	0.1520
21	1.1632	1.0096	0.3631	0.1521
22	1.1782	1.0104	0.3704	0.1531
23	1.1887	1.0106	0.3710	0.1549
24	1.2067	1.0109	0.3743	0.1550
25	1.2255	1.0142	0.3744	0.1555
26	1.2360	1.0159	0.3755	0.1576
27	1.2606	1.0184	0.3768	0.1583
28	1.2618	1.0221	0.3770	0.1585
29	1.2638	1.0227	0.3790	0.1598
30	1.2640	1.0240	0.3795	0.1602
31	1.2662	1.1310	0.3801	0.1602
32	1.2738	1.0316	0.3822	0.1605
33	1.2868	1.0386	0.3823	0.1607
34	1.3015	1.0443	0.3826	0.1608
35	1.3019	1,0479	0.3840	0.1610
36	1.3062	1.0533	0.3856	0,1619
37	1.3168	1.0594	0.3872	0.1631
38	1.3253	1.1612	0.3876	0.1679
39	1.3267	1.0636	0.3910	0.1688
40	1.3322	1.0662	0.3918	0.1696
41	1.3364	1.0663	0.3919	0.1720
42	1.3427	1.0923	0.3925	0.1723
43	1.3467	1.1013	0.4070	0.1737
44	1.3594	1.1020	0.4070	0.1745
45	1.3749	1.1038	0.4073	0.1746

TABLE II - continued

Rank	12.7 ksi	13.0 ksi	14.0 ksi	16.5 ksi
46	1.3785	1.1070	0.4093	0.1747
47	1.3793	1.1130	0.4120	0.1757
48	1.4024	1.1208	0.4121	0.1758
49	1.4035	1.1208	0.4160	0.1767
50	1.4095	1.1428	0.4237	0.1767
51	1.4133	1.1724	0.4243	0.1768
52	1.4135	1.1759	0.4280	0.1790
53	1.4143	1.1773	0.4296	0.1795
54	1.4163	1.1850	0.4350	0.1799
55	1.4348	1.1990	0.4377	0.1806
56	1.4381	1,2013	0.4380	0.1815
57	1.4503	1.2096	0.4390	0.1818
58	1.4510	1.2143	0.4437	0.1822
59	1.4544	1.2211	0.4464	0.1835
60	1.4564	1.2251	0.4470	0.1836
61	1.4572	1.2264	0.4474	0.1839
62	1.4606	1.2289	0.4490	0.1862
63	1.4625	1.2296	0.4504	0.1864
64	1.4638	1.2633	0.4517	0.1866
65	1.4751	1.2662	0.4530	0.1868
66	1.4813	1.2692	0.4544	0.1870
67	1.4815	1.2719	0.4552	0.1881
68	1.4872	1.2761	0.4557	0.1889
69	1.4903	1.2766	0.4580	0.1902
70	1.4977	1.2854	0.4596	0.1907
71	1.5210	1.2882	0.4630	0.1908
72	1.5238	1.2889	0.4632	0.1912
73	1.5299	1,2943	0.4660	0.1930
74	1.5393	1.2957	0.4674	0.1933
75	1.5396	1.3014	0.4702	0.1935
76	1.5439	1.3024	0.4715	0.1935
77	1.5518	1.3032	0.4727	0.1941
78	1.5549	1.3124	0.4733	0.1942
79	1.5570	1.3212	0.4762	0.1947
80	1.5576	1.3259	0.4766	0.1948
81	1.5722	1.3300	0.4766	0.1951
82	1.5773	1.3372	0.4778	0.1980
83	1.5794	1.3389	0.4810	0.1985
84	1.5803	1.3392	0.4832	0.1992
85	1.5847	1.3423	0.4847	0.2001
86	1.5871	1.3461	0.4860	0.2009
87	1.5950	1.3464	0.4913	0.2019
88	1.5952	1.3472	0.4938	0.2019
89	1.6030	1.3474	0.4974	0.2029
90	1.6062	1.3500	0.5004	0.2036
91	1.6140	1.3602	0.5035	0.2041
92	1.6149	1.3609	0.5046	0.2049
93	1.6160	1.3629	0.5053	0.2057

TABLE II - continued

Rank	12.7 ksi	13.0 ksi	14.0 ksi	16.5 ksi
94	1.6210	1.3795	0.5066	0.2065
95	1.6231	1.3836	0.5082	0.2065
96	1.6232	1.3910	0.5112	0.2067
97	1.6256	1.3955	0.5139	0.2067
98	1.6332	1.3988	0.5155	0.2068
99	1.6464	1.4100	0.5180	0.2078
100	1.6497	1.4119	0.5290	0.2083
101	1.6499	1.4212	0.5293	0.2083
102	1.6580	1.4218	0.5320	0.2087
103	1.6625	1.4247	0.5340	0.2106
104	1.6741	1.4469	0.5370	0.2110
105	1.6813	1.4550	0.5500	0.2113
106	1.6872	1.4713	0.5501	0.2114
107	1.6971	1.4794	0.5546	0.2127
108	1.6990	1.4815	0.5549	0.2137
109	1.6992	1.4870	0.5690	0.2145
110	1.6995	1.4970	0.5796	0.2152
111	1.7215	1.4990	0.5830	0.2158
112	1.7236	1.5017	0.5997	0.2165
113	1.7305	1.5100	0.6040	0.2166
114	1.7359	1.5138	0.6050	0.2170
115	1,7551	1.5223	0.6114	0.2171
116	1.7578	1.5351	0.6120	0.2171
117	1.7610	1.5462	0.6279	0.2178
118	1.7762	1.5619	0.6285	0.2178
119	1.7873	1.5620	0.6302	0.2189
120	1.7882	1.5644	0.6332	0.2198
121	1.7940	1.5788	0.6419	0.2205
122	1.8044	1.5819	0.6488	0.2235
123	1.8105	1.5843	0.6600	0.2236
124	1.8473	1.5873	0.6682	0.2241
125	1.8695	1.5874	0.6901	0.2245
126	1.8712	1.5876	0.6940	0.2245
127	1.8809	1.5903	0.7155	0.2249
128	1.8874	1.6201	0.7500	0.2253
129	1.8992	1.6300	0.7524	0.2263
130	1.9152	1.6361	0.7802	0.2289
131	1.9172	1.6532	0.7856	0.2329
132	1.9347	1.6550	0.8179	0.2355
133	1.9484	1.6786	0.8370	0.2358
134	1.9485	1.7536		0.2360
135	1.9604	1.7651		0.2365
136	1.9612	1.7798		0.2371
137	2,0026	1.7825		0.2382
138	2.0171	1.7846		0.2392
139	2.0387	1.8028		0.2392
140	2.0979	1.8279		0.2399
141	2.112	1.8472		0.2400

TABLE II - continued

Rank	12.7 ksi	13.0 ksi	14.0 ksi	16.5 ksi
142	2.1277	1.9292		0.2402
143	2.1348	1.9722		0.2406
144	2.2018	1.9999		0.2407
145	2.2047	2.0782		0.2453
146	2.2103	2.0953		0.2467
147	2.2226	2.1954		0.2467
148	2.2856	2.3850		0.2485
149	2.3502			0.2493
150	2.4582			0.2505
151				0.2514
152				0.2530
153				0.2533
154				0.2542
155				0.2546
156				0.2559
157				0.2565
158				0.2566
159				0.2572
160				0.2586
161				0.2608
162				0.2625
163				0.2632
164				0.2638
165				0.2639
166				0.2648
167				0.2656
168				0.2675
169				0.2712
170				0.2722
171				0.2745
172				0.2751
173				0.2754
174				0.2768
175				0.2779
176				0.2781
177				0.2800
178				0.2802
179				0.2851
180				0.2874
181				0.2877
182				0.2897
183				0.2919
184				0.2927
185				0.2931
186				0.2935
187				0.2944
188				0.3005
189				0.3011

TABLE II - continued

Rank	12.7 ksi	13.0 ksi	14.0 ksi	16.5 ksi
190				0.3020
191				0.3024
192				0.3131
193				0.3141
194				0.3145
195				0.3266
196				0.3318
197				0.3385
198				0.3440
199				0.3453
200				0.3618

TABLE III

PARAMETERS OF SINGLE LOG-NORMAL DISTRIBUTION

	12.7 ksi	13.0 ksi	14.0 ksi	16.5 ksi
Mean of log (N), $\bar{x}$	6.17725	6.10949	5.66479	5.32034
Standard deviation, s	0.099334	0.095913	0.099089	0.102987
Coreelation coeff., r	0.99044	0.99330	0.98726	0.99668

TABLE IV

PARAMETERS OF SINGLE WEIBULL DISTRIBUTION

(CLASSICAL MOMENT METHOD)

	12.7 ksi	13.0 ksi	14.0 ksi	16.5 ksi
Shape parameter, b	2.53	1.76	1.525	2.28
Minimum life, N_o (mill. cycles)	0.62529	0.8046	0.303241	0.105766
Characteristic life, V (mill, cycles)	1.64879	1.38228	0.493641	0.229114
Correlation coefficient, r	0.99554	0.99195	0.96932	0.99654

TABLE V

PARAMETERS OF SINGLE WEIBULL DISTRIBUTION
(UPPER VERTICAL MOMENT METHOD)

	12.7 ksi	13.0 ksi	14.0 ksi	16.5 ksi
Shape parameter, b	3.135	1.819	1.438	2.138
Minimum life, N_o (mill. cycles)	0.59015	0.79284	0.31089	0.11089
Characteristic life, V (mill. cycles)	1.65184	1.38605	0.49197	0.22850
Correlation coefficient, r	0.99649	0.99371	0.99504	0.99828

TABLE VI

PARAMETERS OF THE LOG-NORMAL STF COMPONENT DISTRIBUTION

	12.7 ksi	13.0 ksi	14.0 ksi	16.5 ksi
MEAN life, $\bar{x}$	5.9726	6.0080	5.5715	5.1868
Stand. deviation, s	0.04032	0.03925	0.03835	0.04750
No. of specimens in STF component	14	42	43	38
Correlation coefficient, r		0.98419	0.98088	0.9894

TABLE VII

PARAMETERS OF THE WEIBULL LTF COMPONENT DISTRIBUTION

	12.7 ksi	13.0 ksi	14.0 ksi	16.5 ksi
Shape parameter, b	1.827	1.444	1.068	1.625
Minimum life, N_o (mill. cycles)	1.084	1.086	0.417	0.158
Characteristic life, V (mill. cycles)	1.648	1.486	0.541	0.238
Mean of N, $\bar{N}$ (mill. cycles)	1.607	1.447	0.538	0.226
Mean of log (N), $\bar{x}$	6.1994	6.1543	5.7241	5.3462
Stand. dev. of log (N)	0.07429	0.07203	0.07508	0.08440
Correlation coeff., r	0.99837	0.98527	0.99096	0.99584
Estimated no. of specimens in LTF component distribution (no. of spec. having $N \geq N_o$)	136	107	84	165
Percent LTF of total	90.6	71.0	62.4	82.5

APPENDIX A

The One-Sided Truncated Log-Normal Distribution

If, in a given distribution the number and corresponding values of the observations below (or above) a certain value, the truncation point are known, the distribution is said to be truncated. If the number of the observations of unspecified values is known the distribution is called censored. If, however, the two parameters $\bar{x}$ and s^2 of the normal distribution are known the probabilities can be calculated at any point in the distribution. The parameters may be estimated by the method of maximum likelihood. Hald has in Ref. 18 given the procedure for estimating the parameters of a one-sided truncated distribution in which the truncation point and the values above that point are known.

The point of truncation is taken as origin, i.e. if X_1, X_2, ... X_n are the observed endurances then $x_i = X_i - X_{tr}$ is the variable (X_{tr} is the truncation point).

The procedure is first to calculate

$$y = \frac{n_{tr} \sum_{i=1}^{n} x_i^2}{2\left(\sum_{i=1}^{n} x_i\right)^2} \qquad \text{(A. 1)}$$

From Table I in Ref. 18 an estimate of the standardised point of truncation z, is found as $z = f(y)$.

Using Table II to find $g(z)$, we further compute the estimate of the standard deviation as

$$s = g(z) \frac{1}{n_{tr}} \sum_{i=1}^{n} x_i \qquad \text{(A. 2)}$$

and the estimate of the mean is

$$\bar{x} = -zs \qquad \text{(A. 3)}$$

The degree of truncation (the percentage of unknown observations in the population) is $P(z)$ where P is the cumulative normal distribution function in the Notation.

The above method is directly applicable whether the known observations are above or below the point of truncation, provided the requirement $x > 0$ is satisfied.

APPENDIX B

The Weibull (Extreme Value) Distribution

Assuming that in a large group of specimens tested at the same stress amplitude and subjected to a number N of load cycles, the specimen that actually fails at this number is necessarily the weakest specimen, one may consider those specimens failing at the lowest number of cycles as forming a group of the weakest specimens within the population from which the sample is drawn. The theory of extreme values may therefore be applied to the distribution of N.

The theory of extreme values leads to the following probability distribution function (Ref. 13):

$$F_1(N) = 1 - \exp\left[-(N/V)^b\right] \qquad \text{(B. 1)}$$

with boundary conditions

$$F_1(0) = 1, \qquad F_1(\infty) = 0$$

i. e. the probability of survival approaches 100% as N approaches zero, and approaches zero as N approaches infinity.

It is well known that fatigue, for virgin specimens, is a gradual (consecutive) chain of developments. It has also been found that the damaging process in the early stages can be either directly reversible (e. g. "annealing out damage") or indirectly reversible (e. g. localized damage inhibited by hardening of the surrounding matrix) thus yielding a "healing effect.

On this basis it is reasonable to assume a lower bound, N_o, for the endurance N below which no failure can occur. This leads to the following modification of the probability distribution function given in Eq. (B. 1).

$$F(N) = 1 - \exp\left\{-\left[(N-N_o) / (V-N_o)\right]^b\right\} \qquad \text{(B. 2)}$$

The parameters N_o (the "minimum life") and V (the "characteristic life") are defined by the probabilities

$$F(N \leq N_o) = 0$$

and

$$F(V) = 1/e$$

The frequency distribution function associated with F(N) is

$$f(N) = \frac{b}{(V-N_o)}\left[\frac{N-N_o}{V-N_o}\right]^{b-1} \times \exp\left\{-\left[(N-N_o)/(V-N_o)\right]^b\right\} \qquad \text{(B. 5)}$$

Using the method of moments due to Weibull (Ref. 14), Freudenthal and Gumbel have in Ref. 13 given a method for calculating the three parameters N_o, b and V directly without iteration procedures.

According to Ref. 13, the shape parameter b is defined by the "skewness", $\sqrt{\beta_1}$:

$$\sqrt{\beta_1} = \left[\Gamma(1+3/b) - 3\Gamma(1+2/b)\Gamma(1+1/b) + 2\Gamma^3(1+1/b)\right] \times \left[\Gamma(1+2/b) - \Gamma^2(1+1/b)\right]^{-3/2} \quad \text{(B. 6)}$$

The skewness is given by the third central moment μ_3 and the standard deviation σ as

$$\sqrt{\beta_1} = \mu_3 \sigma^{-3} \quad \text{(B. 7)}$$

$\sqrt{\beta_1}$ is estimated by the sample value

$$\sqrt{\beta_1} = \frac{\sqrt{n(n-1)}}{n-2} \quad \frac{\bar{N}^3 - 3\bar{N}^2\bar{N} + 2\bar{N}^3}{(\bar{N}^2 - \bar{N}^2)^{3/2}} \quad \text{(B. 8)}$$

and b is then calculated from Eq. (B. 6).

The sample standard deviation s is obtained by the usual formula

$$s = \sqrt{\frac{\sum_{i=1}^{n} (N_i - \bar{N})}{n-1}} \quad \text{(B. 9)}$$

The characteristic life V is given by

$$V = N + \sigma A(b) \quad \text{(B. 10)}$$

and the minimum life N_o by

$$N_o = V - \sigma B(b) \quad \text{(B. 11)}$$

where

$$A(b) = \left[1 - \Gamma(1+1/b)\right]\left[\Gamma(1+2/b) - \Gamma^2(1+1/b)\right]^{-1/2} \quad \text{(B. 12)}$$

and

$$B(b) = \left[\Gamma(1+2/b) - \Gamma^2(1+1/b)\right]^{-1/2} \quad \text{(B. 13)}$$

Replacing the population standard deviation σ with the sample value s, and using the previously obtained value of b, A(b) and B(b) can be calculated with the use of tables of the gamma function. V and N_o are then calculated from Eqs. B. 10 and B. 11.

In the derivation of the above equations the classical method of moments of Weibull (Refs. 14 and 15) was used. To distinguish it from

the method of upper vertical moments (Appendix C), the above method will hereafter be referred to as "the classical moment method".

APPENDIX C

The Truncated Weibull (Extreme Value) Distribution

Weibull (Ref. 16) has given a method for calculating the parameters of complete, cencored and truncated distributions by the method of upper vertical moments.

The upper vertical moment of order r is defined by

$$\bar{x}_r = \int_{x_a}^{x_b} \left[1 - P(x)\right]^r dx \qquad \text{(C. 1)}$$

In the Weibull (or Extreme Value) distribution

$$F(N) = 1 - \exp\left\{- \left[(N-N_o)/(V-N_o)\right]^b\right\} \qquad \text{(C. 2)}$$

the parameters N_o, b and V are obtained by solving

$$\begin{aligned} \bar{x}_1 &= N_o + \frac{V-N_o}{b} \Gamma(1/b)\, I\left[u_1,\ (1/b - 1)\right] \\ \bar{x}_2 &= N_o + \frac{V-N_o}{b2^{1/b}} \Gamma(1/b)\, I\left[u_2,\ (1/b - 1)\right] \\ \bar{x}_3 &= N_o + \frac{V-N_o}{b2^{2/b}} \Gamma(1/b)\, I\left[u_4,\ (1/b - 1)\right] \end{aligned} \qquad \text{(C. 3)}$$

where Γ is the complete gamma-function, $I\left[u_r,\ (1/b - 1)\right]$ is an integral introduced and tabulated by Pearson (Ref. 17). The integral is defined as

$$I(u,\ p) = \frac{1}{\Gamma(p+1)} \int_o^{u\sqrt{p+1}} e^{-y}\, y^p\, dy \qquad \text{(C. 4)}$$

u_r is given by

$$u_r = \sqrt{b}\ (\ln \frac{1}{1-P_r})^{1/b} \qquad \text{(C. 5)}$$

and

$$P_r = 1 - (1-P)^r \qquad \text{(C. 6)}$$

Since for a complete distribution

$$I\left[\infty,\ (\frac{1}{b} - 1)\right] = 1 \qquad \text{(C. 7)}$$

and since

$$\Gamma(1 + 1/b) = 1/b\, \Gamma(1/b) \qquad \text{(C. 8)}$$

Eqs. C. 3 take the simpler form

$$\bar{x}_1 = N_o + \frac{V-N_o}{b} \Gamma(1/b)$$

$$\bar{x}_2 = N_o + \frac{V-N_o}{b} \Gamma(1/b) \qquad \text{(C. 9)}$$

$$\bar{x}_4 = N_o + \frac{V-N_o}{b} \Gamma(1/b)$$

Taking the same degree of truncation, $(1-P_t)$, for each of Eq. (C. 3), Eq. (C. 5) shows that $u_1 = u_2 = u_4$. It then follows that

$$\frac{x_1 - N_o}{x_2 - N_o} = \frac{\bar{x}_2 - N_o}{\bar{x}_4 - N_o} = 2^{1/b} \qquad \text{(C. 10)}$$

from which the shape parameter b is obtained as

$$b = \frac{\log 2}{\log (\bar{x}_1 - N_o) - \log (\bar{x}_2 - N_o)} \qquad \text{(C. 11)}$$

and

$$N_o = \frac{\bar{x}_1 \bar{x}_4 - \bar{x}_2}{\bar{x}_1 + \bar{x}_4 - 2\bar{x}_2} \qquad \text{(C. 12)}$$

The first equation of Eq. (C. 3) then gives

$$V = N_o + \frac{\bar{x}_1 - N_o}{\Gamma(1/b)\, I[u_1, (1/b-1)]} \qquad \text{(C. 13)}$$

An estimate of the moment $\bar{x}_r$ can be obtained from

$$\bar{x}_r = (1-\bar{P}_i)^r (N_{i+1} - N_i) + N_i \qquad \text{(C. 14)}$$

$$\bar{P}_i = 1/2 (P_i + P_{i+1}) \qquad \text{(C. 15)}$$

and P_i is the plotting position.

While the three parameters in the case of a complete distribution may be calculated by the use of Tables of the gamma function and Pearson's integral from Eqs. (C. 9) and Eq. (C. 13) using Eq. (C. 14) to estimate the moments, it is simpler to use Eq. (C. 11) and (C. 12) to obtain b and N_o. By a suitable transformation of Eq. (C. 2), V can be calculated by regression analysis.

Linearising Eq. (C. 2) by taking the natural logarithm of both sides, we get

$$\ln \left(\frac{1}{1-P}\right)^{1/b} = \frac{N - N_o}{V-N_o} \qquad \text{(C. 16)}$$

and, introducing

$$z = \ln \left(\frac{1}{1-P}\right)^{1/b} \qquad \text{(C. 17)}$$

into Eq. (C. 16), we get

$$N = N_o + z\,(V - N_o) \tag{C. 18}$$

Regression by the method of least squares now gives

$$V = N_o + \frac{n\sum Nz - N\sum z}{n\sum z^2 + (\sum z)^2} \tag{C. 19}$$

Eqs. (C. 11) and (C. 12) are independent of the degree of truncation and are thus valid for complete as well as for censored or truncated distributions. Another advantage of using Eqs. (C. 11), (C. 12) and (C. 19) is that they are particularly suited for computation by electronic digital computers.

APPENDIX D

Linear Regression Analysis

The term regression analysis is used for the statistical analysis of the association between two (or more) variables. An important application is to fit a straight line to a set of experimental data points. One method is to minimize the sum of the squares of the deviations of the data points from the line to be fitted to the points. The estimate of the parameters for the line obtained by this method are "best" in the sense that they are normally distributed with the parameters as mean values and with least possible variances (Ref. 19). The deviations are assumed to be normally distributed and their variance constant. With these assumptions the method of least squares is equivalent to the method of maximum likelihood (Ref. 22). The method of linear estimators (Ref. 12), in which the basic assumptions are more general (e.g. normality of the distribution of the dependent variable is not assumed), leads to exactly the same estimates of the parameters.

In fitting a linear equation

$$y - y_o = M_L (x - x_o) \tag{D. 1}$$

to the set of experimental points $(x_i - y_i)$ the parameters M, x_o and y_o have to be determined. If there are no requirements concerning the point (x_o, y_o), the least squares method gives the following estimates of the parameters.

$$\begin{aligned} x_o &= \bar{x} \qquad \text{i.e. the mean of } x_i \\ y_o &= \bar{y} \qquad \text{i.e. the mean of } y_i \end{aligned} \tag{D. 2}$$

(Expressions for $\bar{x}$ and $\bar{y}$ are found in the Notation).

The slope of the regression line is then given by

$$M_L = \frac{\sum_{i=1}^{n} (x_i - \bar{x})\, y_i}{\sum_{i=1}^{n} (x_i - \bar{x})^2} = \frac{n \sum_{i=1}^{n} x_i y_i - \sum_{i=1}^{n} x_i \sum_{i=1}^{n} y_i}{n \sum_{i=1}^{n} x_i^2 - \left(\sum_{i=1}^{n} x_i \right)^2} \tag{D. 3}$$

The correlation coefficient, r, characterizes the dependence between the variables x and y, i.e. in the case of fitting a straight line to experimental points, r is an overall measure of how well the points fit the regression line. r is the ratio between the covariance, sxy, and the produce of the standard deviations of the two variables (see Notation), and is thus given by

$$r = \frac{\sum_{i=1}^{n} (x_i - \bar{x}) \quad (y_i - \bar{y})}{\sum_{i=1}^{n} (x - \bar{x})^2 \sum_{i=1}^{n} (y - \bar{y})^2} \quad 1/2 \tag{D. 4}$$

The values r may assume are in the range

$$-1 \leq r \leq 1$$

For $r = \pm 1$, all points lie on the line indicating a complete correlation. For $r = 0$ there is no correlation, i.e. the variables are stochastically independent. The theory for the correlation coefficient is only valid if the errors are normally distributed (Ref. 19), and the interpretation of r is very uncertain if this requirement is not satisfied. In the case of regression on the probability plots (Section 4), the assumption of normally distributed variables seems to hold; visual comparisons show that the best fit to the regression line is in all cases coincident with the highest correlation coefficients.

Linear regression analysis is directly applicable to a function linearized by any arbitrary transformation provided the variance of the transformed dependent variable is constant. For a logarithmic transformation this is a rather dubious assumption and some bias in the estimates may result.

In this work regression analysis has been used to fit a straight line to the plots of the endurances on probability paper. The choice of plotting position is of some importance since biased estimates of the parameters may result if a poor choice of plotting position is made, especially if the sample is small.

The most used plotting positions are

$$P = (i - 1/2) / n \qquad \text{(D. 5)}$$

and

$$P = i / (n+1) \qquad \text{(D. 6)}$$

An improved plotting position is given by Blom (Ref. 20) as

$$P = \frac{i - \alpha}{n - \alpha + \beta + 1} \quad (0 \leq \alpha, \beta \leq 1) \qquad \text{(D. 7)}$$

where α and β are chosen with regard to the distribution. For a normal distribution the plotting position

$$P = (i - 3/8) / (n + 1/4) \qquad \text{(D. 8)}$$

gives a nearly unbiased estimate of the variance (Ref. 12).

For large numbers of observations, say $n > 100$, the difference between the various plotting positions is negligible. For practical purposes the plotting relation given by Eq. (D. 8) was used for all plots. In the regression analysis of the Weibull distribution, however, the plotting position (D. 6) was tried. The results did not differ significantly from those obtained using (D. 8).

APPENDIX E

Stresses in the Fatigue Specimen Due to Grip Misalignment

During final assembly of the machine a straingauged steel specimen (see Section 2.5) was used to ensure grip alignment. It was found, however, that the stress in this specimen could not be completely eliminated, and the following calculations were carried out to asses the magnitude of the stresses in the fatigue specimen caused by the grip misalignment. The procedure is to use the strain readings obtained from the alignment specimen to calculate the angular and translational displacement of the grips with respect to each other and use these values to compute the stresses in the fatigue specimen.

The deformation of the specimen caused by grip misalignment can be split into the two following components:

a) A translational displacement, i.e. the centre lines of the gripped ends of the specimen remain parallel, but are displaced a distance δ .
b) An angular or rotational displacement, i.e. the gripped ends are rotated through an angle α , but are not displaced otherwise.

In the first case the deformation and the resulting bending moment diagram are as shown in the following sketch

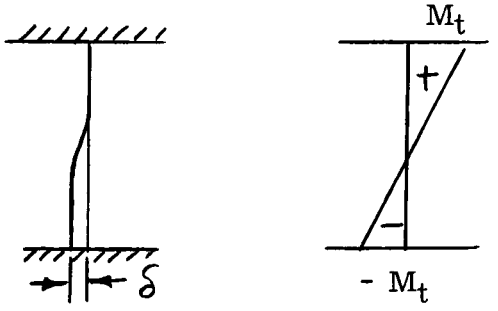

The relation between the displacement d and the maximum value of the bending moment is (Ref. 23),

$$M_t = \frac{6\,EI\delta}{\ell^2} \qquad \text{(E. 1)}$$

Pure angular displacement gives rise to the following deformation and moment diagram (considering the top end as a reference)

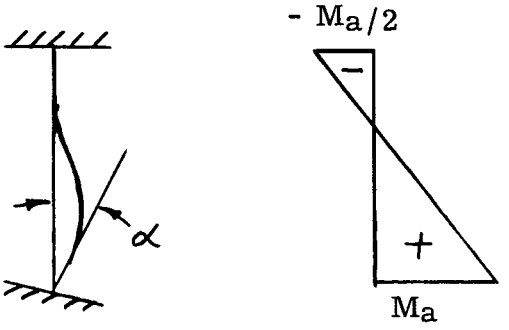

The value of the bending moment at the lower end is (Ref. 23):

$$M_a = \frac{6\ EI\alpha}{l} \qquad \text{(E. 2)}$$

In the general case, when there is a combination of the two deformations, the deformation and the moment diagram are:

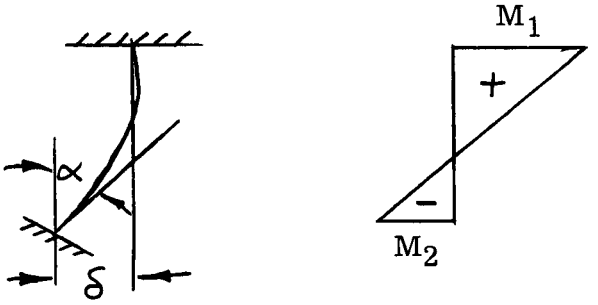

The moments M_t, M_a and M_1 and M_2 are related as follows

$$M_1 = M_t - 1/2\ M_a$$
$$M_2 = -M_t + M_a \qquad \text{(E. 3a)}$$

or

$$M_a = 2\ (M_1 + M_2)$$
$$M_t = 2\ M_1 + M_2 \qquad \text{(E. 3b)}$$

The strain readings can be used to calculate M_1 and M_2,, but not directly since the gauges were located at a distance from the ends. The sketch shows how the moments at the gauges, M_1' and M_2', and the end moments M_1 and M_2 are related.

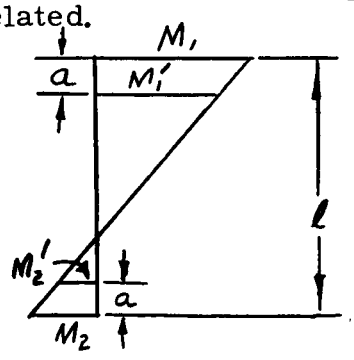

Simple geometrical considerations lead to the following expressions for the end moments

$$M_1 = \frac{(\ell - a)\, M_1' - a M_2'}{\ell - 2a}$$

$$M_2 = \frac{(\ell - a)\, M_2' - a M_1'}{\ell - 2a} \qquad \text{(E. 4)}$$

Using the well-known equations $\epsilon = \frac{\sigma_b}{E}$

and $\sigma_b = \frac{M}{I} y = \frac{M}{Z}$

the bending moment at the gauges may be expressed as

$$M' = \epsilon' E Z$$

or, using the previous notation

$$M_1' = \epsilon_1' E Z$$
$$M_2' = \epsilon_2' E Z \qquad \text{(E. 5)}$$

The readings of the bending strains were obtained by clamping the specimen in the grips, adjusting the mean stress spring and the upper head until there was no axial load in the specimen, and take one set of readings from all gauge pairs. Then the specimen was released, rotated 90 degrees, clamped again and a new set of readings taken. This was repeated until the specimen was rotated through 360 degrees and four sets of readings obtained. The readings were taken in this manner to avoid errors due to initial curvature of the alignment specimen. Although the time between alignment checks was up to three months no significant changes were found.

In the last check the following average readings were obtained:

	Long. plane	Transverse plane
Top end	+ 32	+ 3
Bottom end	- 60	+ 3

The readings are in microinch per inch (μ in./in.) For bending in the longitudinal plane, the minus sign occurs when the surface strain at the front of the specimen is tensile. Since the bending strains in the transverse plane are very small compared to those in the longitudinal plane, only bending in the latter plane need be considered.

The two gauges on opposite faces at each cross section were wired in adjacent arms in a Wheatstone bridge, giving readings of twice the actual strain. Therefore, the actual strains are

$$\epsilon_1' = +\ 32/2 \quad = 16\,\mu \text{ in./in.}$$

$$\epsilon_2' = -\ 60/2 \quad = 30\,\mu \text{ in./in.}$$

Eq. (E. 5) gives the bending moments at the gauges:

$$M_1' = 27.3 \text{ lb. in.}$$

$$M_2' = -51.4 \text{ lb. in.}$$

The end moments M_1 and M_2 are then computed, using Eq. (E. 4):

$$M_1 = 53.5 \text{ lb. in.}$$

$$M_2 = -81.6 \text{ lb. in.}$$

Using Eq. (E. 3b) the "translational" and "angular" moments are calculated:

$$M_t = 25.4 \text{ lb. in.}$$

$$M_a = -56.2 \text{ lb. in.}$$

The translational displacement of one grip with respect to the other is then (from Eq. (E. 1)):

$$\delta = 0.79 \times 10^{-4} \text{ in.}$$

The angular displacement is given by Eq. (E. 2)

$$\alpha = -\ 0.55 \times 10^{-4} \text{ radians}$$

The moments in the fatigue specimen caused by these displacements are found by equating the expressions for the displacements for the two specimens. Denoting the alignment specimen by subscript a and the fatigue specimen by subscript f, then

$$g = \frac{M_{ta}\, \ell_a^2}{6E_a I_a} = \frac{M_{tf}\, \ell_f^2}{6E_f I_f}$$

i.e.

$$M_{tf} = \frac{E_f I_f}{E_c I_c} \left(\frac{\ell_a}{\ell_f}\right)^2 M_{ta}$$

and similarly

$$M_{af} = \frac{E_f I_f}{E_c I_c} \quad \frac{\ell_a}{\ell_f} M_{a_a}$$

Substituting the numerical values for E, I and 1 we get

$$M_{tf} = 1.99 \text{ lb. in.}$$

$$M_{af} = -1.57 \text{ lb. in.}$$

Eq. A. 3 now gives the moments at the ends of the test section

$$M_{1f} = 2.78 \text{ lb. in.}$$

$$M_{2f} = -3.56 \text{ lb. in.}$$

The stresses at the upper and lower end of the test section of the fatigue specimen may now be calculated using the usual formula for the bending stress at the surface, viz.

$$\sigma_B = \frac{M}{Z}$$

Thus we obtain

$$\sigma_{B_1} = 1160 \text{ psi}$$

$$\sigma_{B_2} = -1490 \text{ psi}$$

Since the minus sign indicates tensile stress at the front of the specimen, the maximum tensile surface stress is at the lower front fillet.

APPENDIX F

Temperature Increase in the Fatigue Specimens During the Test

In fatigue tests conducted at room temperatures it is usually assumed that the temperature rise in the test piece is constant for all stress amplitudes or so small that it can be neglected. This may not always be true; in some cases the temperatures developed in the specimen at high stress amplitudes are so high that a S-N curve determined from such tests is based on endurances which have actually been measured at different temperatures.

The temperature rise is a measure of the energy dissipated during fatiguing of the specimen, i.e. it is a measure of the width of the hysteresis loop. Some energy is stored during the fatigue process (Ref. 24) however, the stored energy is a small fraction of the total energy. A number of factors such as internal damping, heat transfer properties of the material, stress distribution and frequency and amplitude of the applied load determine the temperature rise.

Energy dissipation in the specimen may be measured in two ways: by measuring the amount of heat produced, e.g. by attaching a thermocouple to the specimen, or by measuring the damping in the specimen. Since the second method is less direct and has the disadvantage that the measured energy loss in most cases would include energy lost in the grips, etc., the thermocouple method was preferred.

To ensure good heat conduction the thermocouple was soldered to a piece of thin copper sheet, curved to fit the waisted part of the specimen. The copper piece and the thermocouple were covered with a 1/16 in. layer of plastic to minimize heat loss to the air. A heat-conducting grease was used to further enhance heat transfer to the thermocouple. The reference thermocouple was attached to the machine structure (assumed to remain at room temperature throughout the test), so that the active thermocouple only recorded temperatures above the room temperature. The temperature was recorded continuously during the test but because the virgin specimens were very soft the energy loss was large in the beginning of the test and full operating stress was not reached until about 4000 cycles, therefore the readings before this number of cycles are not included. The temperature increase (above room temperature) vs. number of cycles is plotted in Fig. 18 for typical specimens from the four stress levels.

The curves for the specimens tested at the two lowest stress amplitudes, 12.7 ksi and 13.0 ksi, show that once the initial hardening was over, the amount of dissipated energy remained small during the greater part of the test with a small increase toward the end. The energy dissipated in the specimens tested at the higher stresses, 16.5 ksi and 14.0 ksi, increased steadily during the test, indicating a continuing

widening of the hysteresis loop. The same trend is reported in Ref. 25. Since most of the energy is dissipated in slip zones, the observed temperature increase is a measure of the severity of the slip. This is confirmed bythe metallographic examination of the failed specimens in Ref. 8, which showed that gross deformation took place with the grains breaking up into cells (H-type fatigue damage) at the highest stress, while at the lowest stress damage was confined to slip bands (F-type fatigue damage).

The relatively small amounts of heat developed in the specimens (the maximum temperature above the room temperature was about 17 deg. F) leads to the assumption that the heating of the specimen had little or no effect on the observed fatigue endurances.

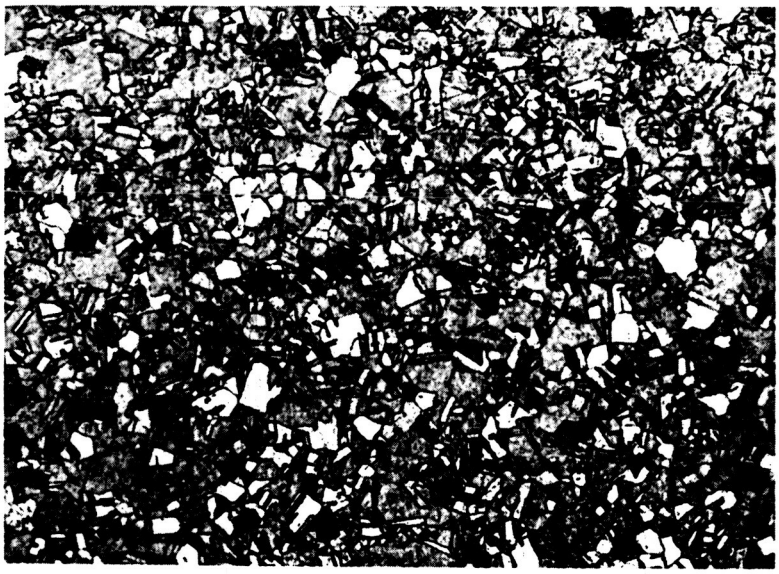

FIG. 1 TYPICAL TRANSVERSE SECTION OF SPECIMEN BEFORE TESTING. ASTM GRAIN SIZE NO. 8 (x 100)

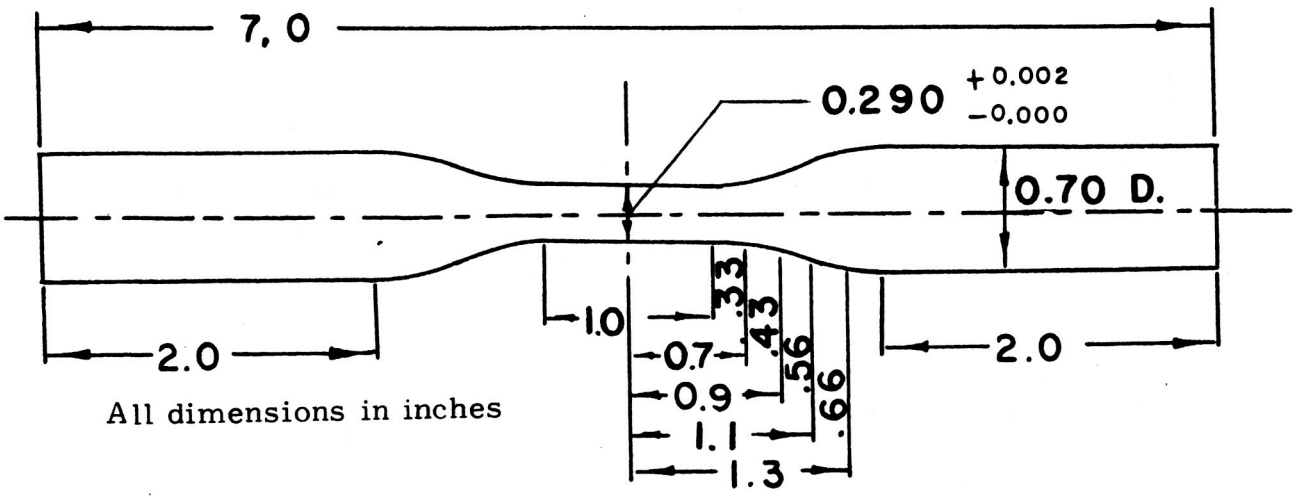

FIG. 2 THE COPPER (OFHC) FATIGUE SPECIMEN

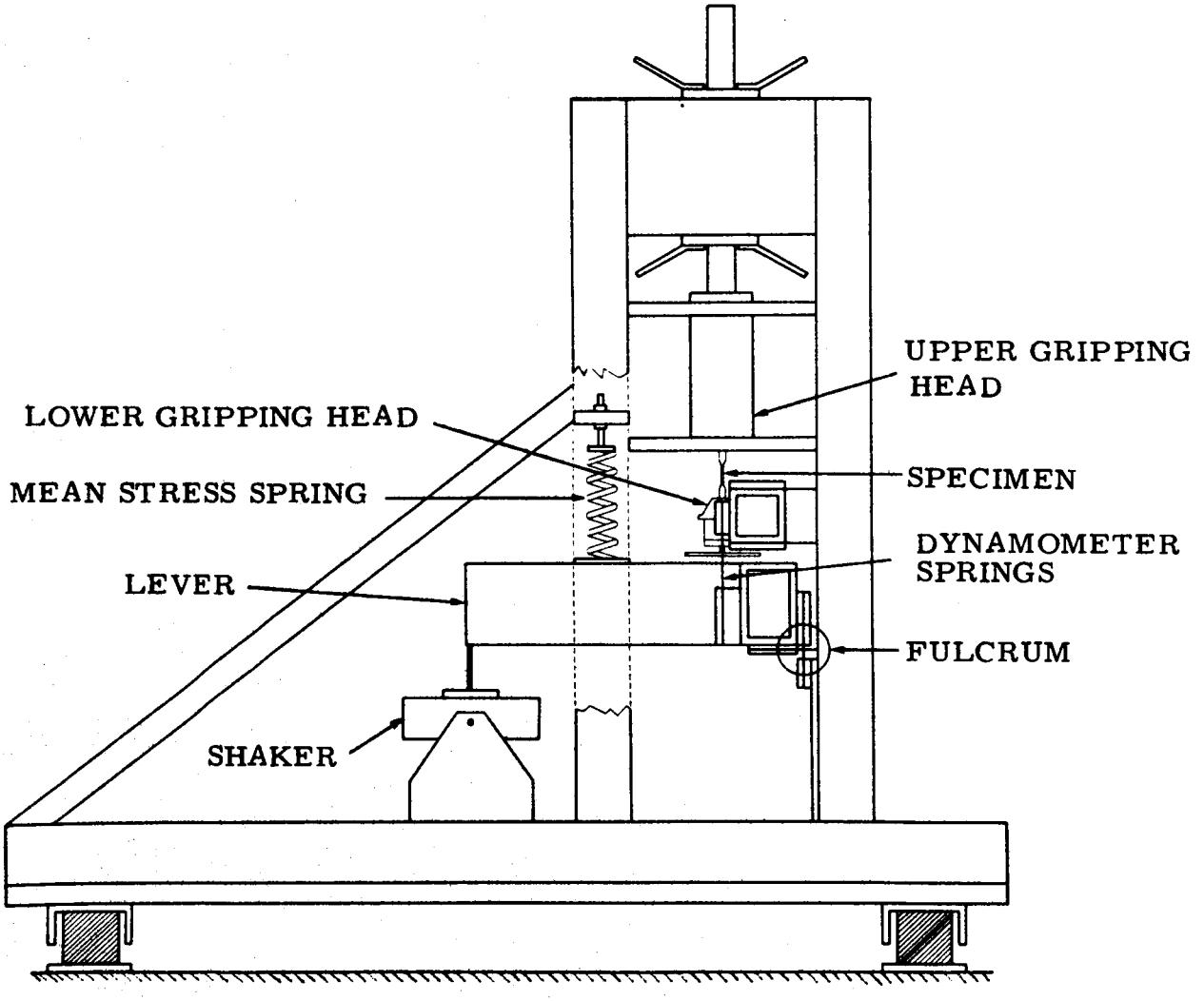

FIG. 3 THE FATIGUE MACHINE (SCHEMATIC).

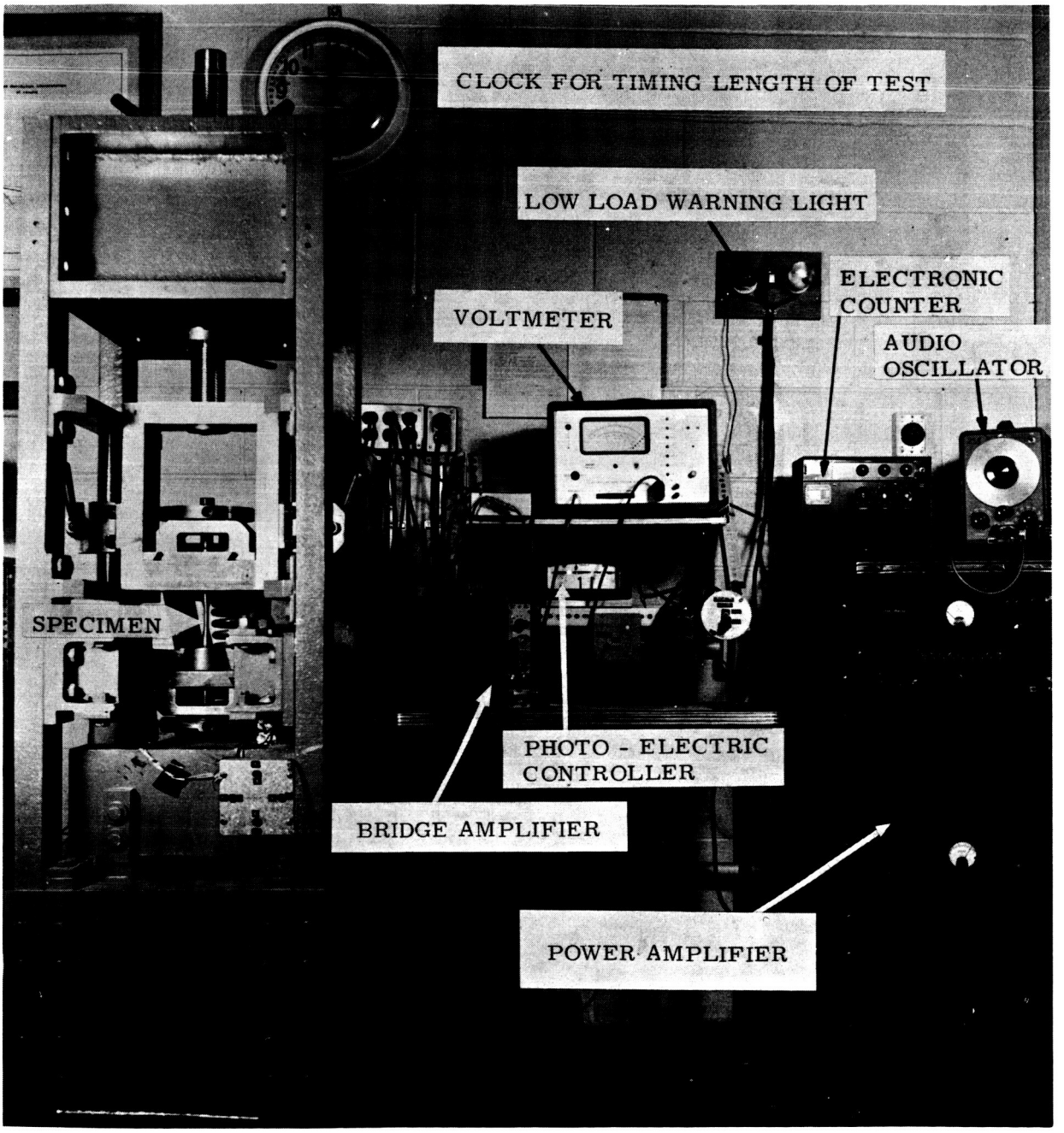

FIG. 4 THE FATIGUE MACHINE WITH INSTRUMENTS

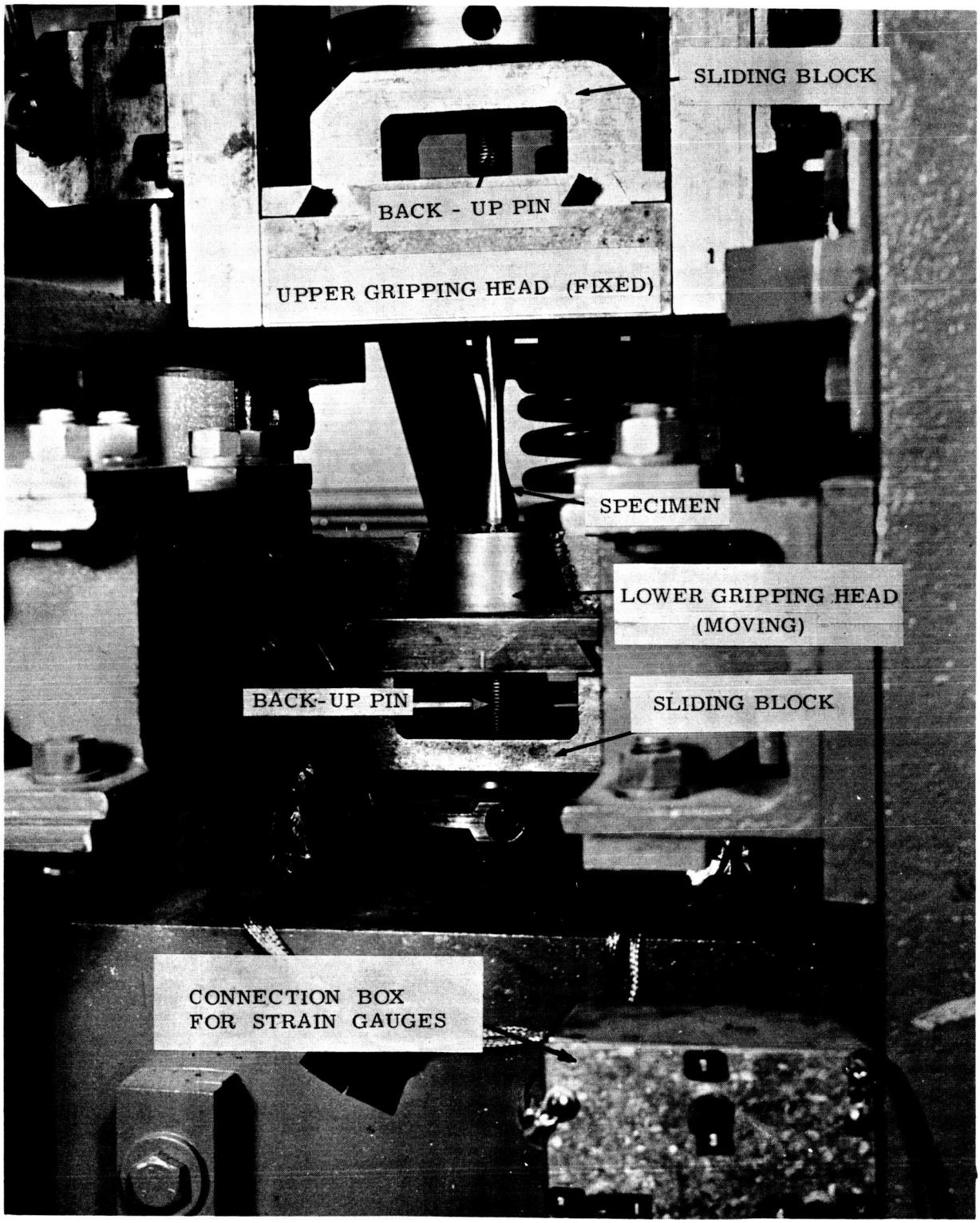

FIG. 5 (a) FRONT VIEW OF THE FATIGUE MACHINE SHOWING GRIPPING HEADS

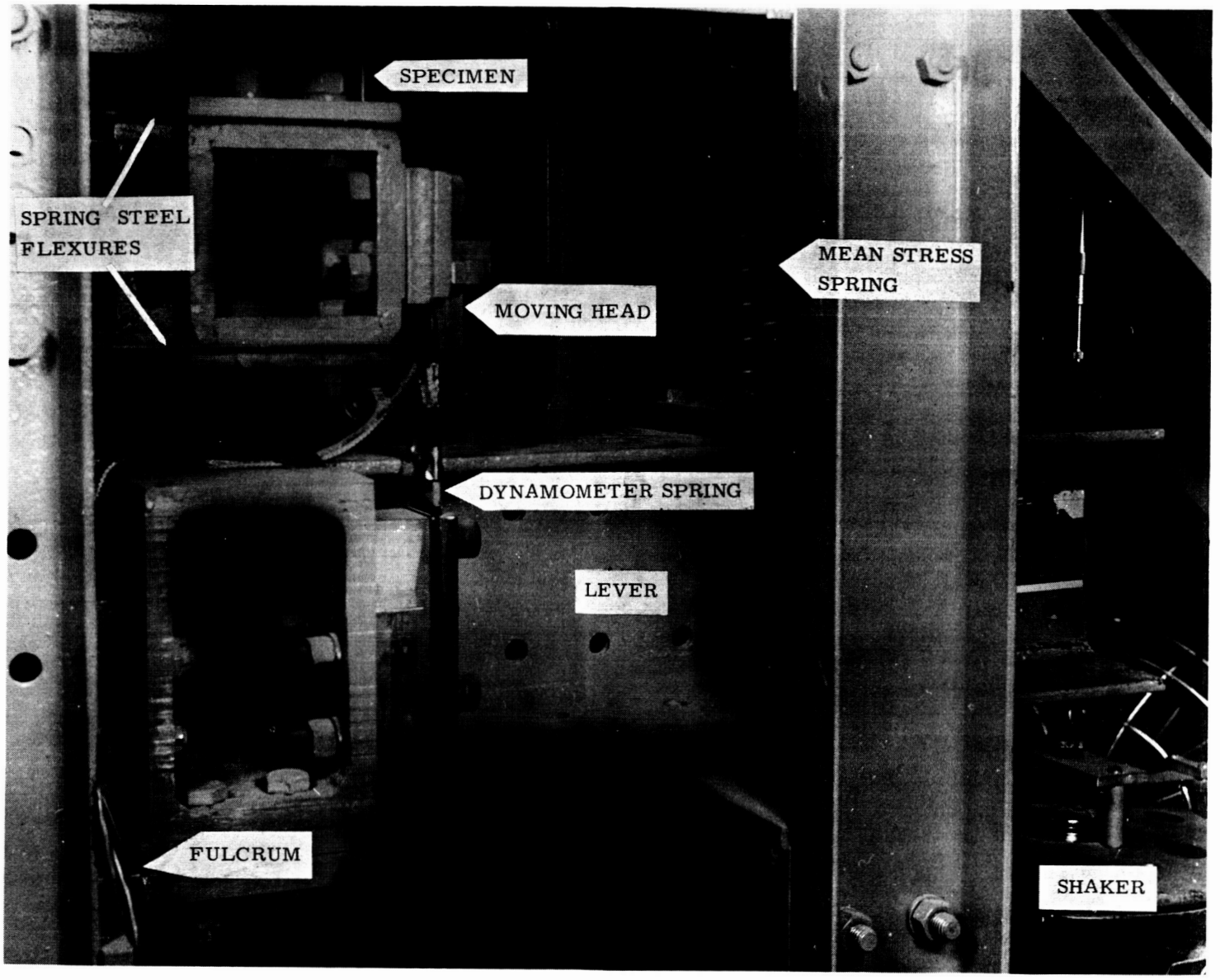

FIG. 5 (b) SIDE VIEW OF FATIGUE MACHINE SHOVING MOVING PARTS

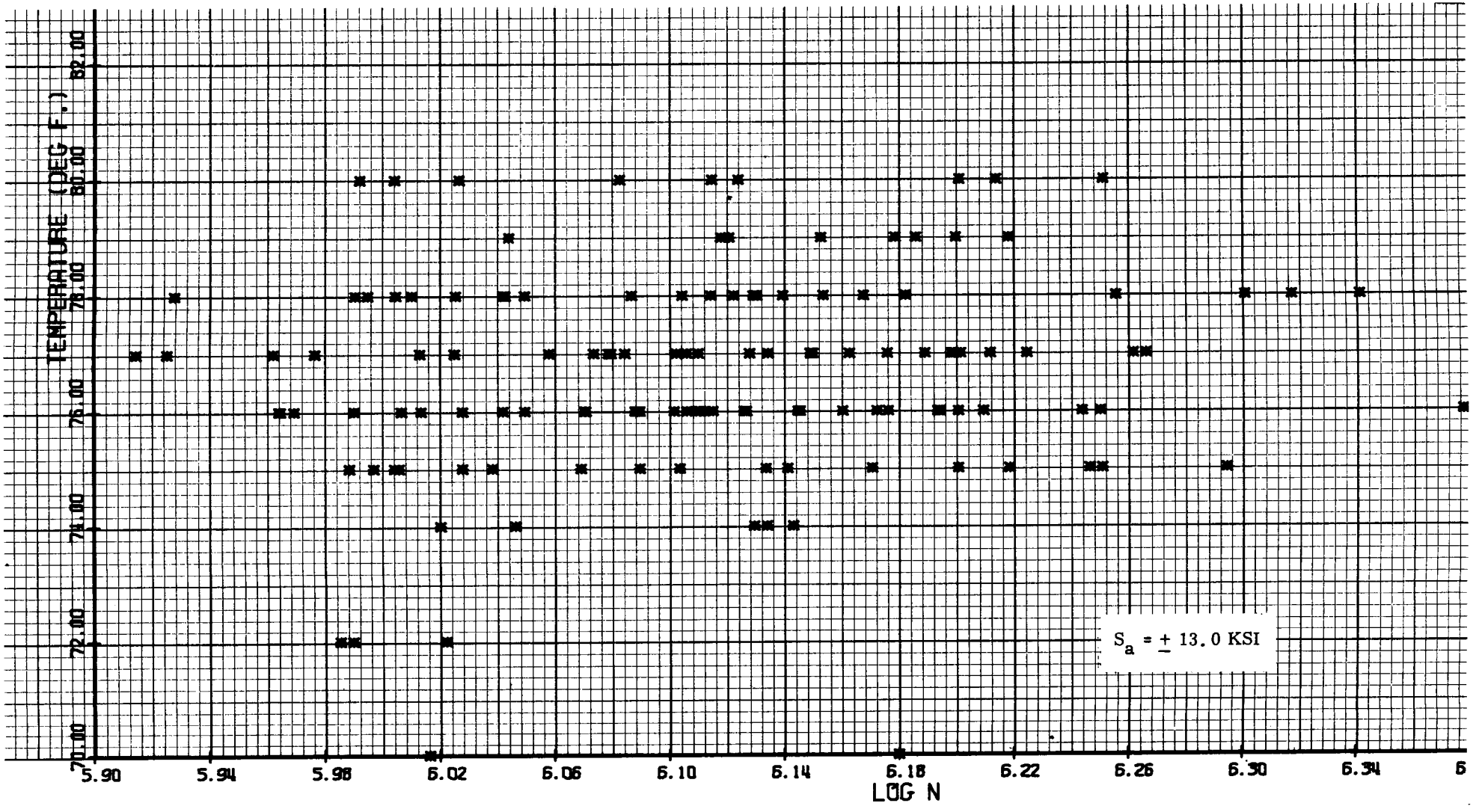

FIG. 6 (a) TEMPERATURE VS. LOG N

TOP

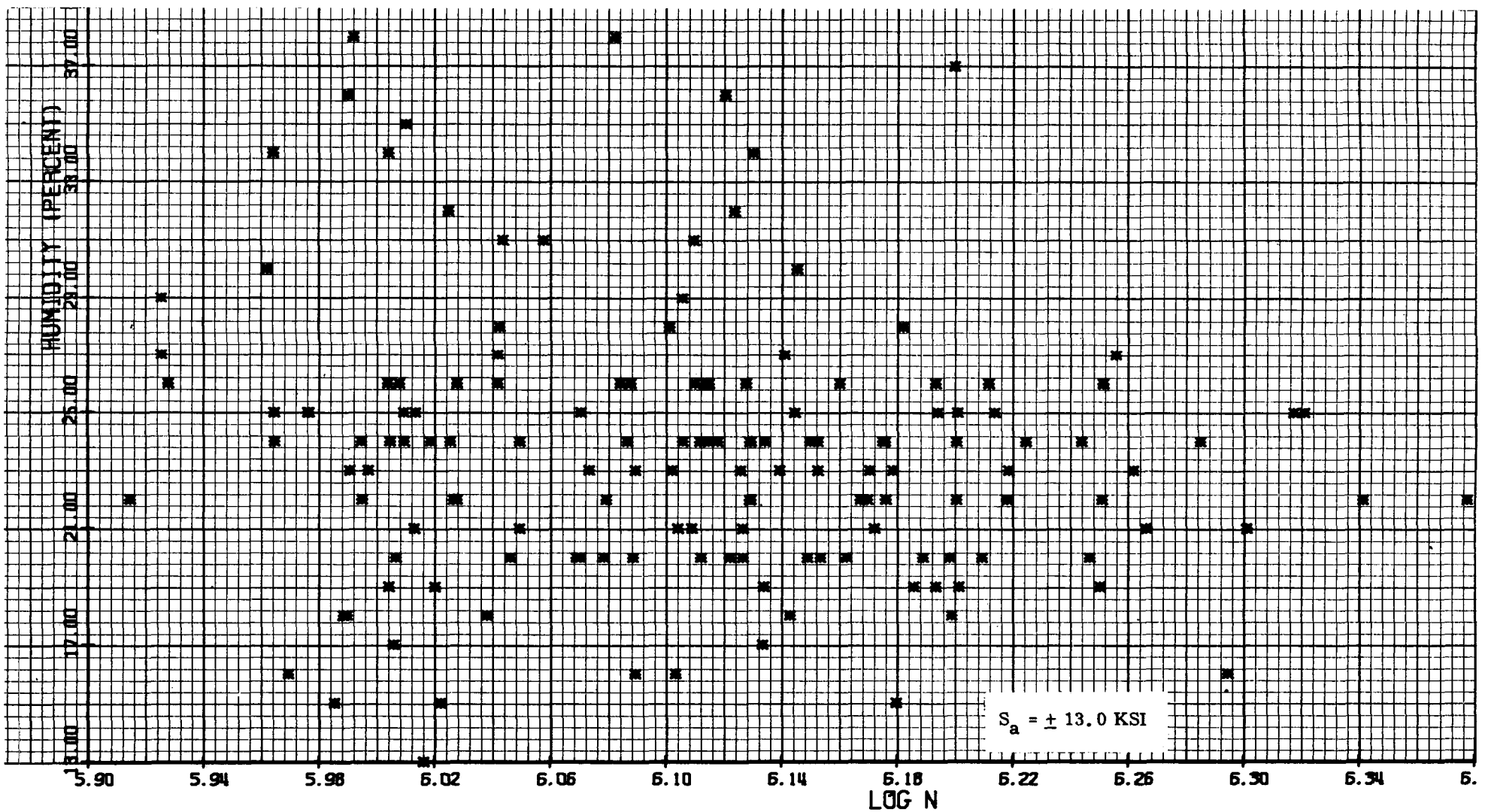

FIG. 6 (b) HUMIDITY VS. LOG N

TOP

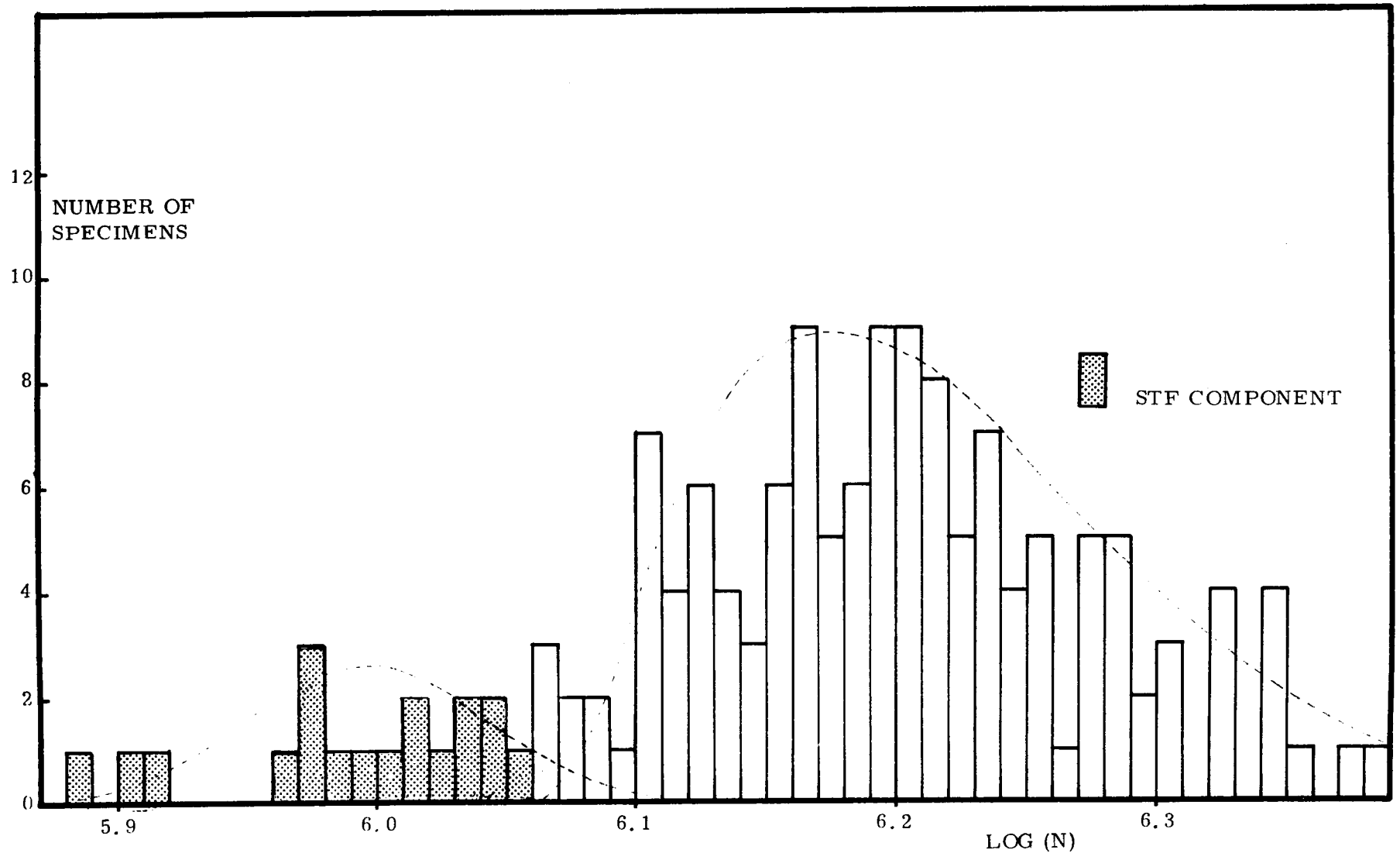

FIG. 7 (a) HISTOGRAM
Stress amplitude : $\pm$ 12.7 ksi
Number of specimens : 150
Class length : 0.01 log(N)

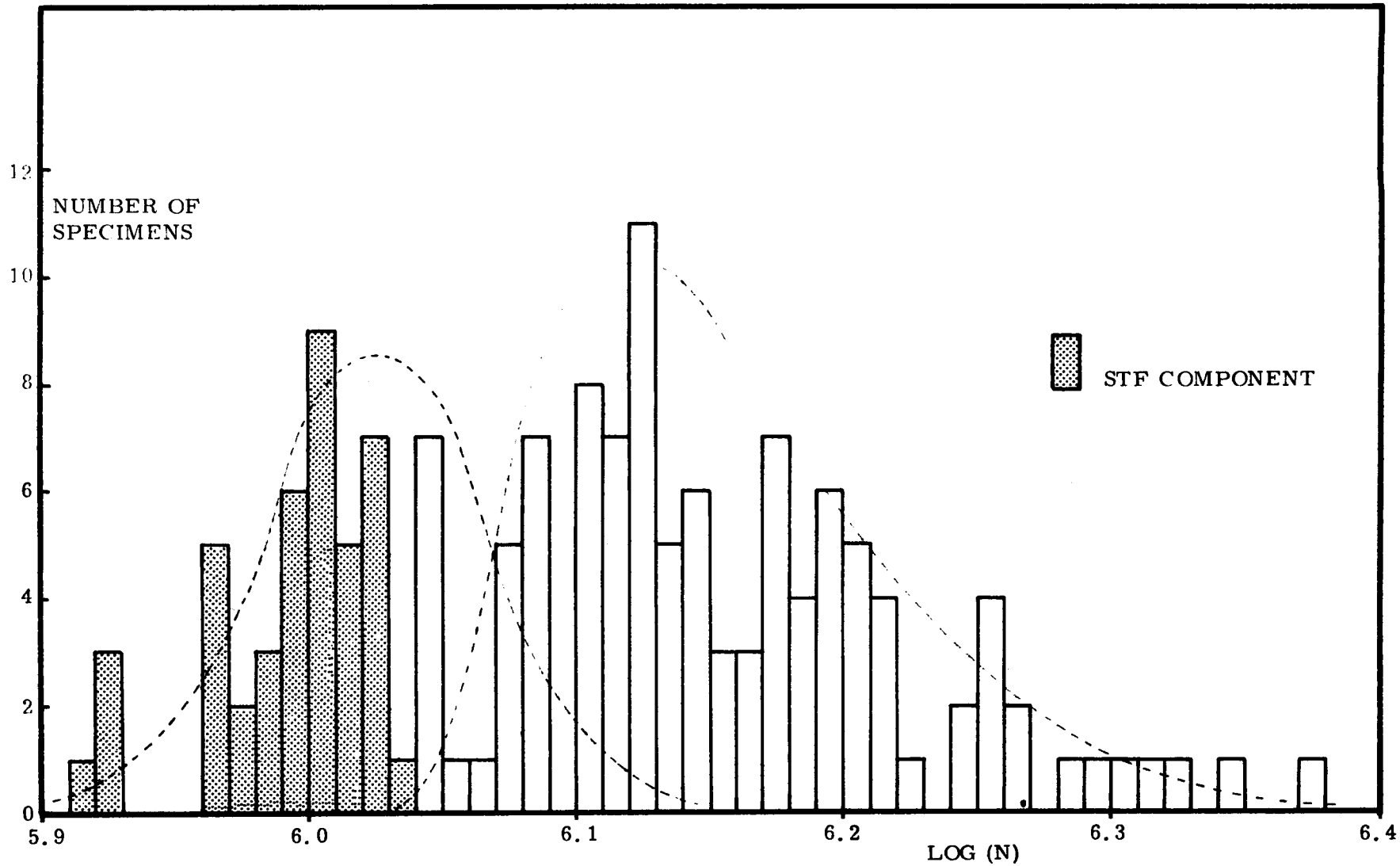

FIG. 7 (b) HISTOGRAM
Stress amplitude : $\pm$ 13.0 ksi
Number of specimens : 148
Class length : 0.01 log(N)

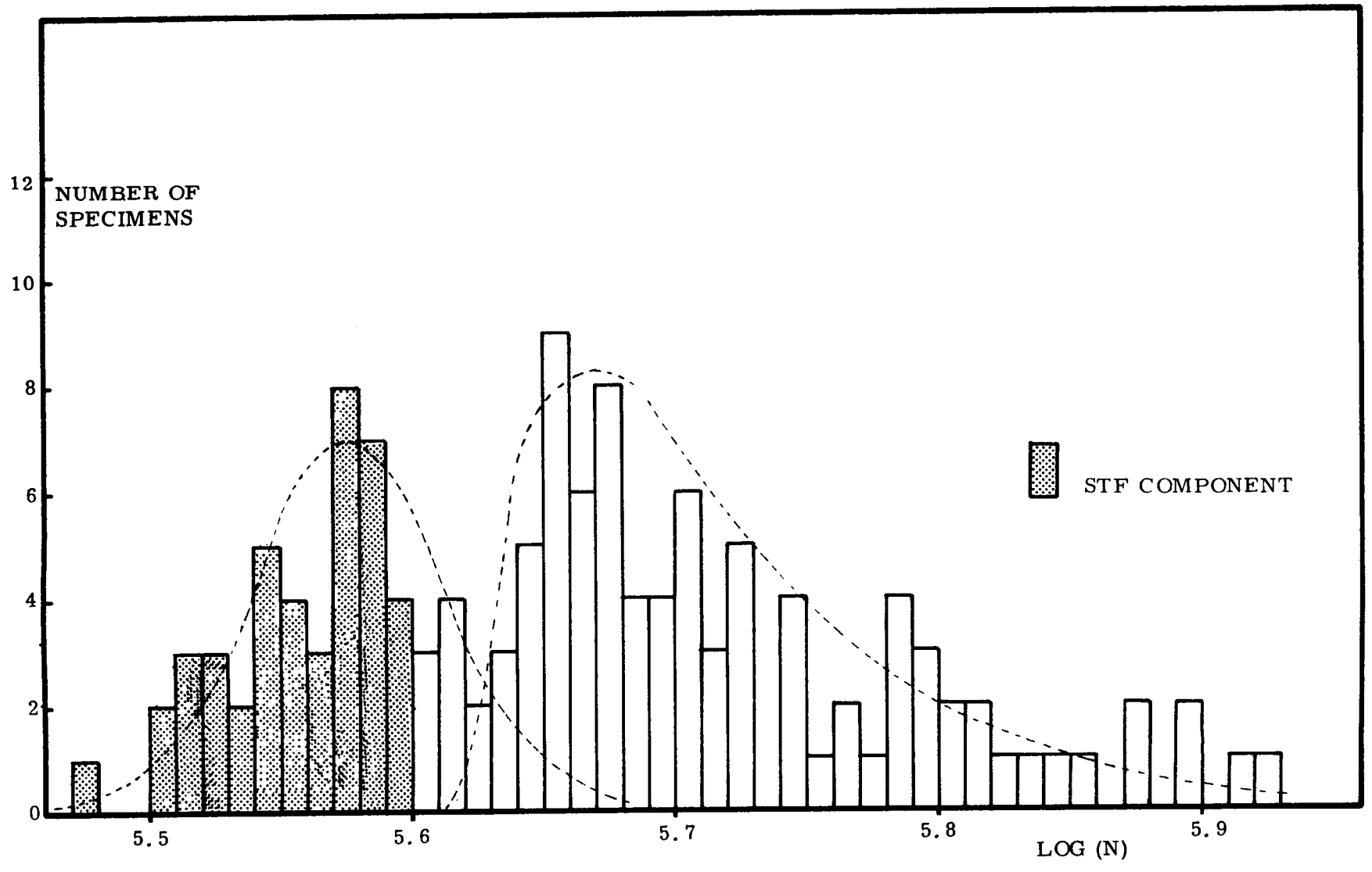

FIG. 7 (c) HISTOGRAM
Stress amplitude : $\pm$ 14.0 ksi
Number of specimens : 133
Class length : 0.01 log(N)

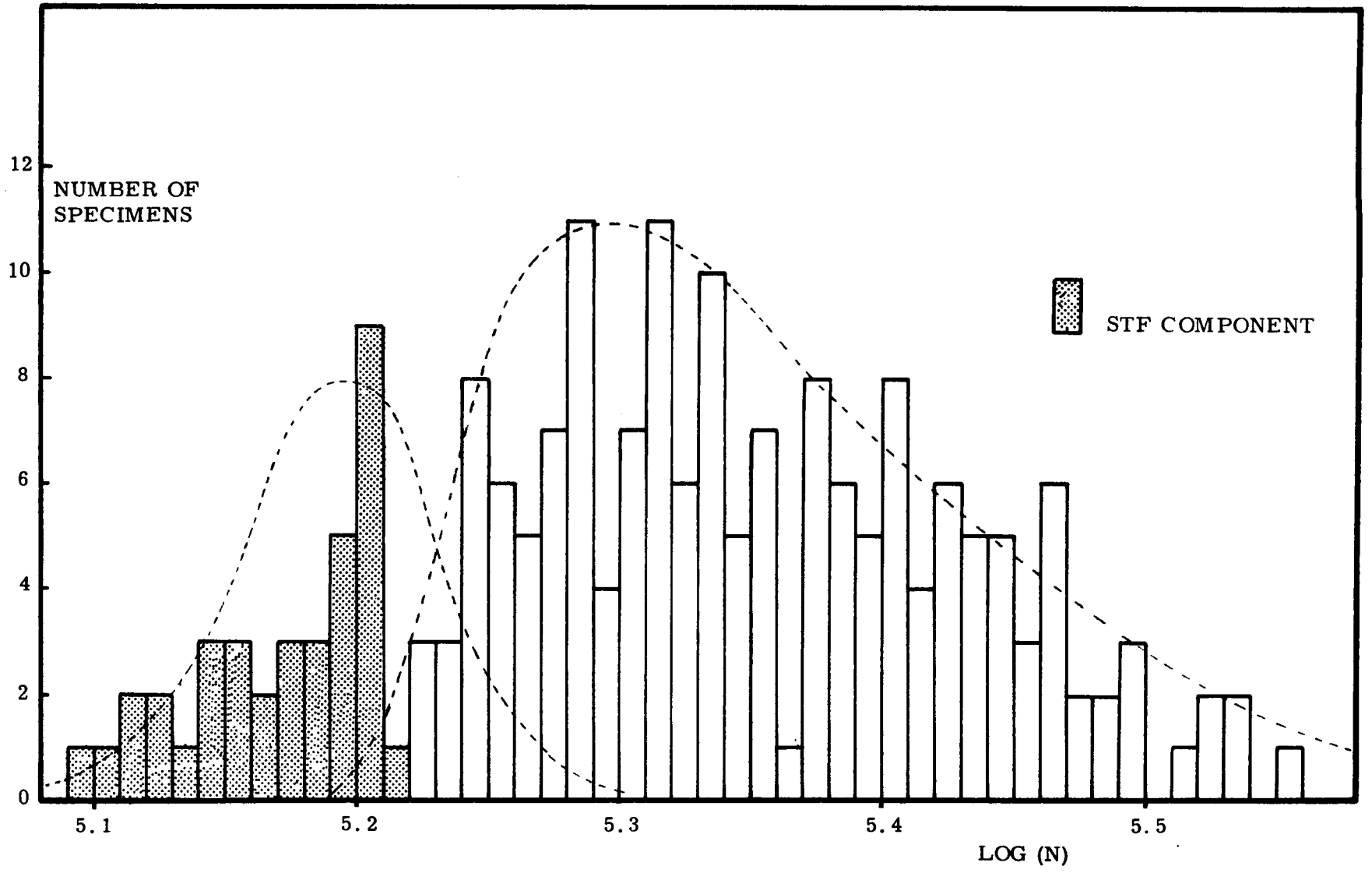

FIG. 7 (d) HISTOGRAM
Stress amplitude : ± 16.5 ksi
Number of specimens : 200
Class length : 0.01 log(N)

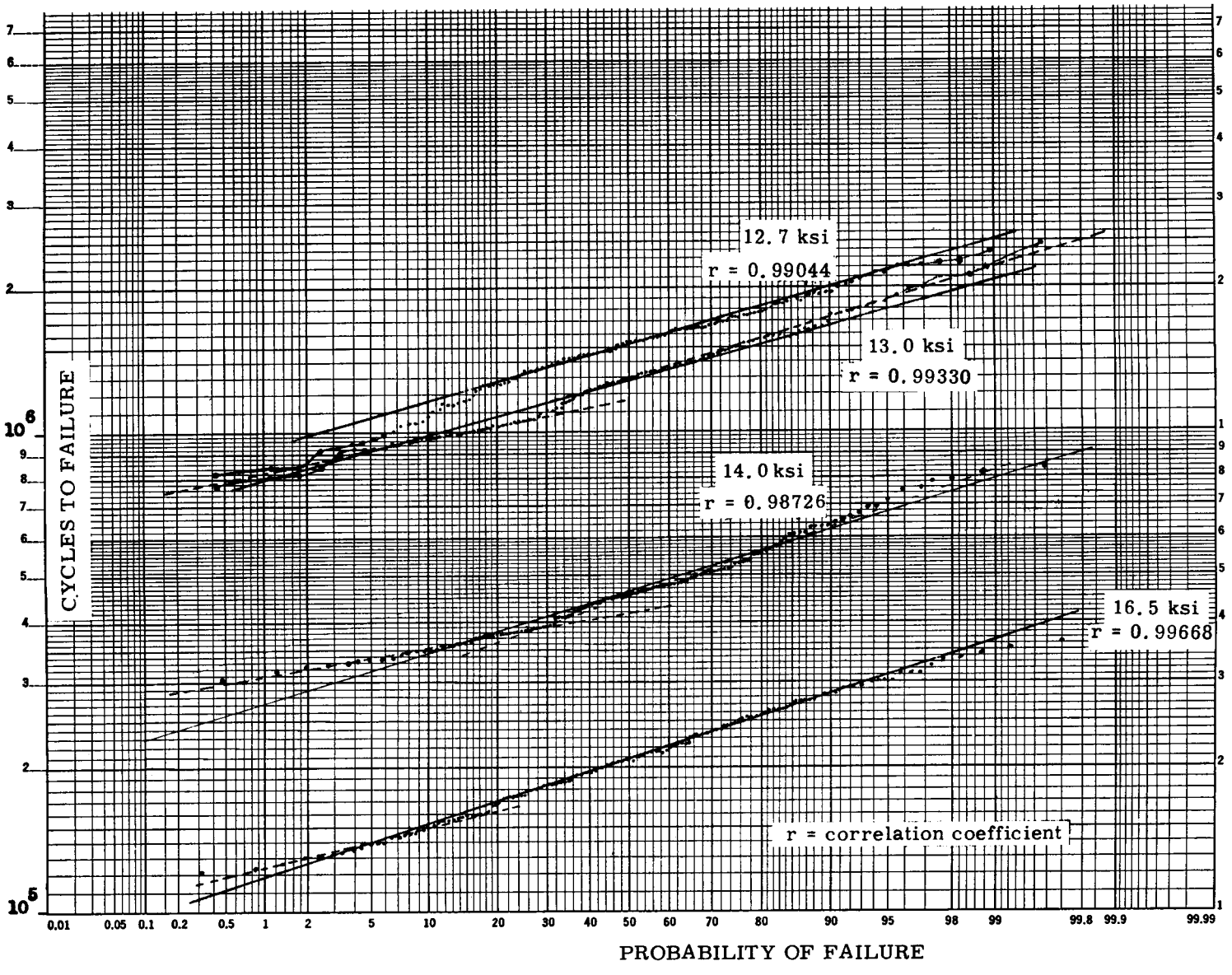

FIG. 8 LOG-NORMAL PROBABILITY PLOT, SINGLE DISTRIBUTION

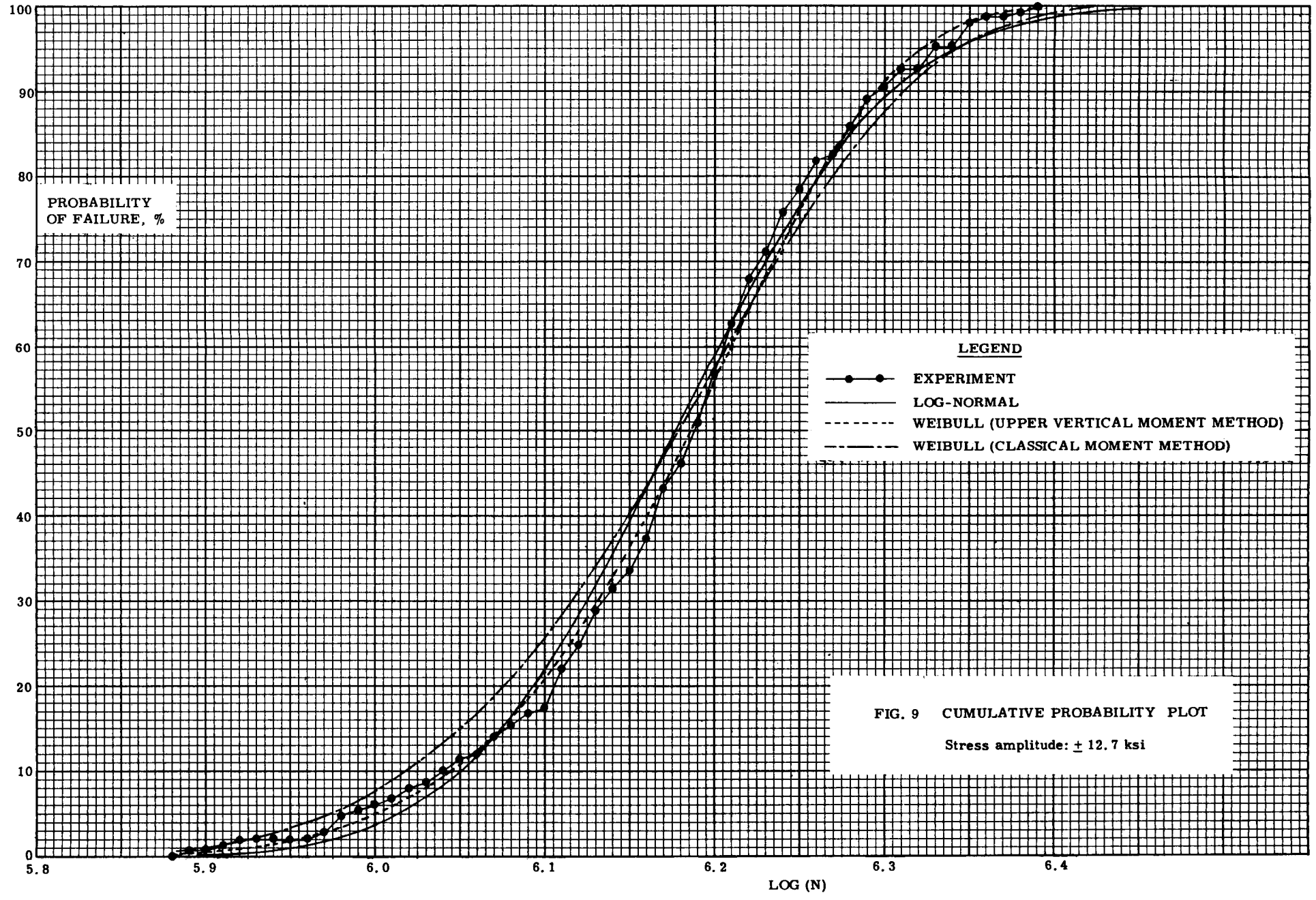

FIG. 9 CUMULATIVE PROBABILITY PLOT

Stress amplitude: $\pm$ 12.7 ksi

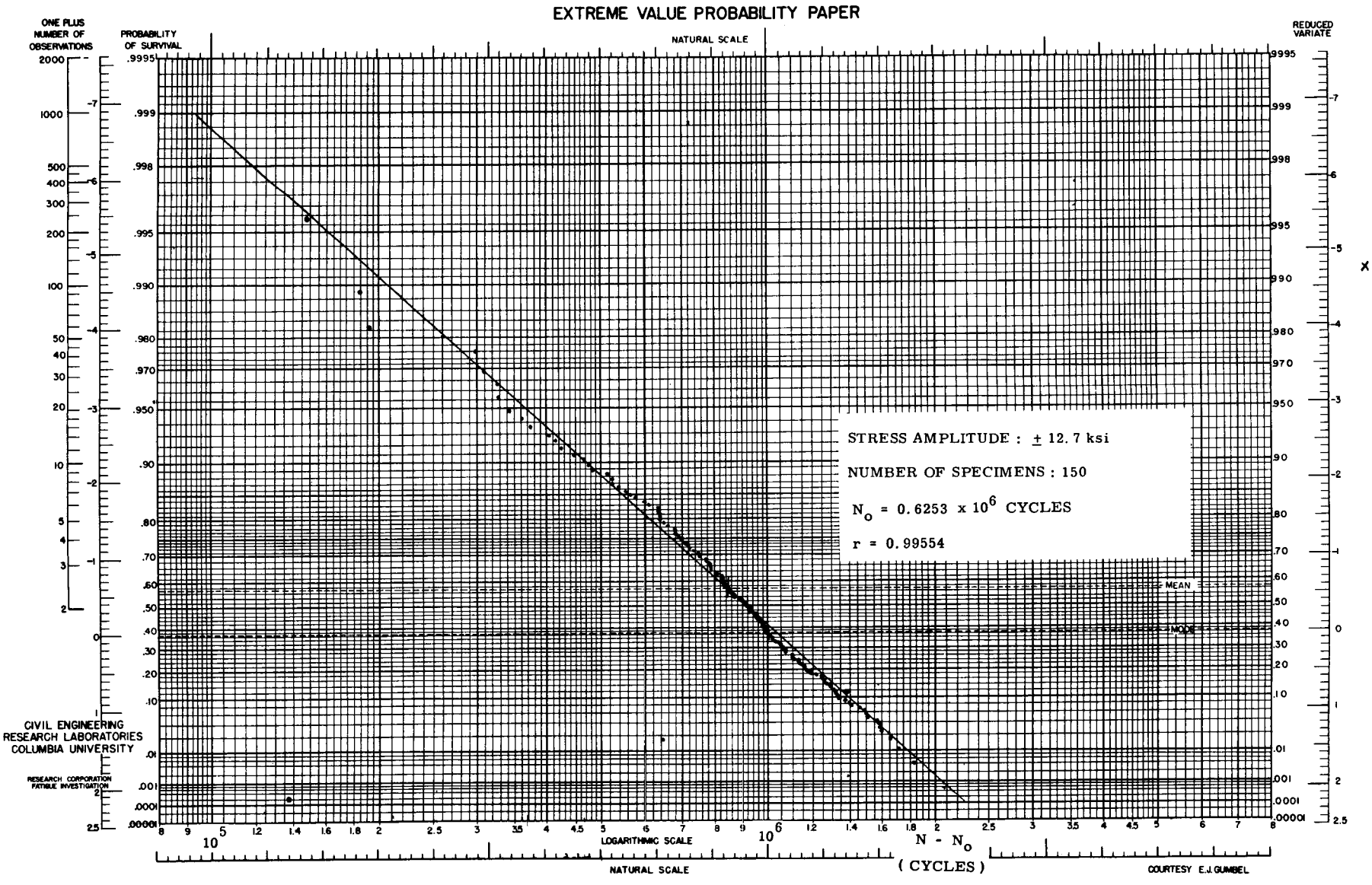

FIG. 10 (a) WEIBULL PROBABILITY PLOT, SINGLE DISTRIBUTION. PARAMETERS CALCULATED BY THE CLASSICAL MOMENT METHOD.

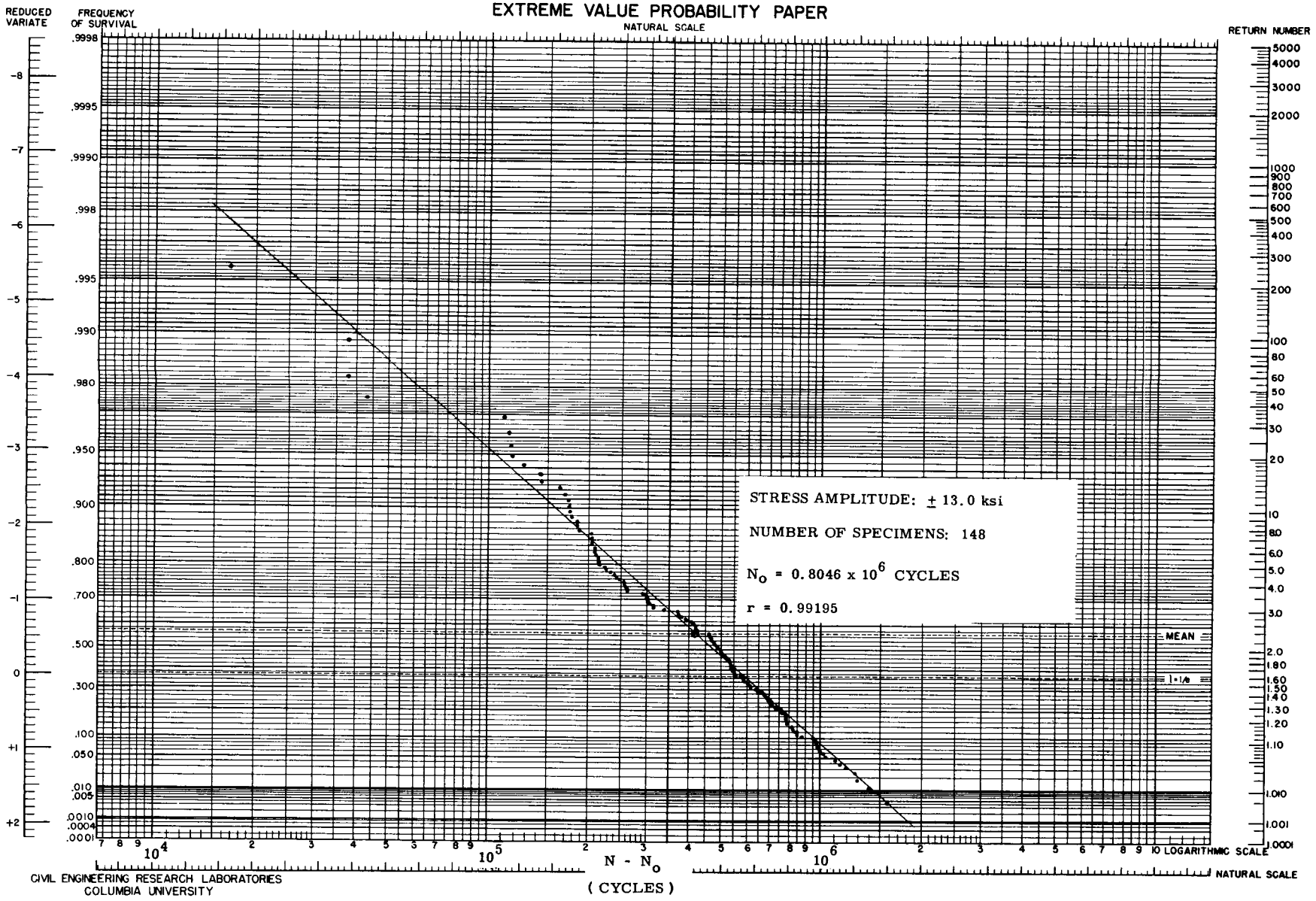

FIG. 10 (b) WEIBULL PROBABILITY PLOT, SINGLE DISTRIBUTION. PARAMETERS CALCULATED BY THE CLASSICAL MOMENT METHOD.

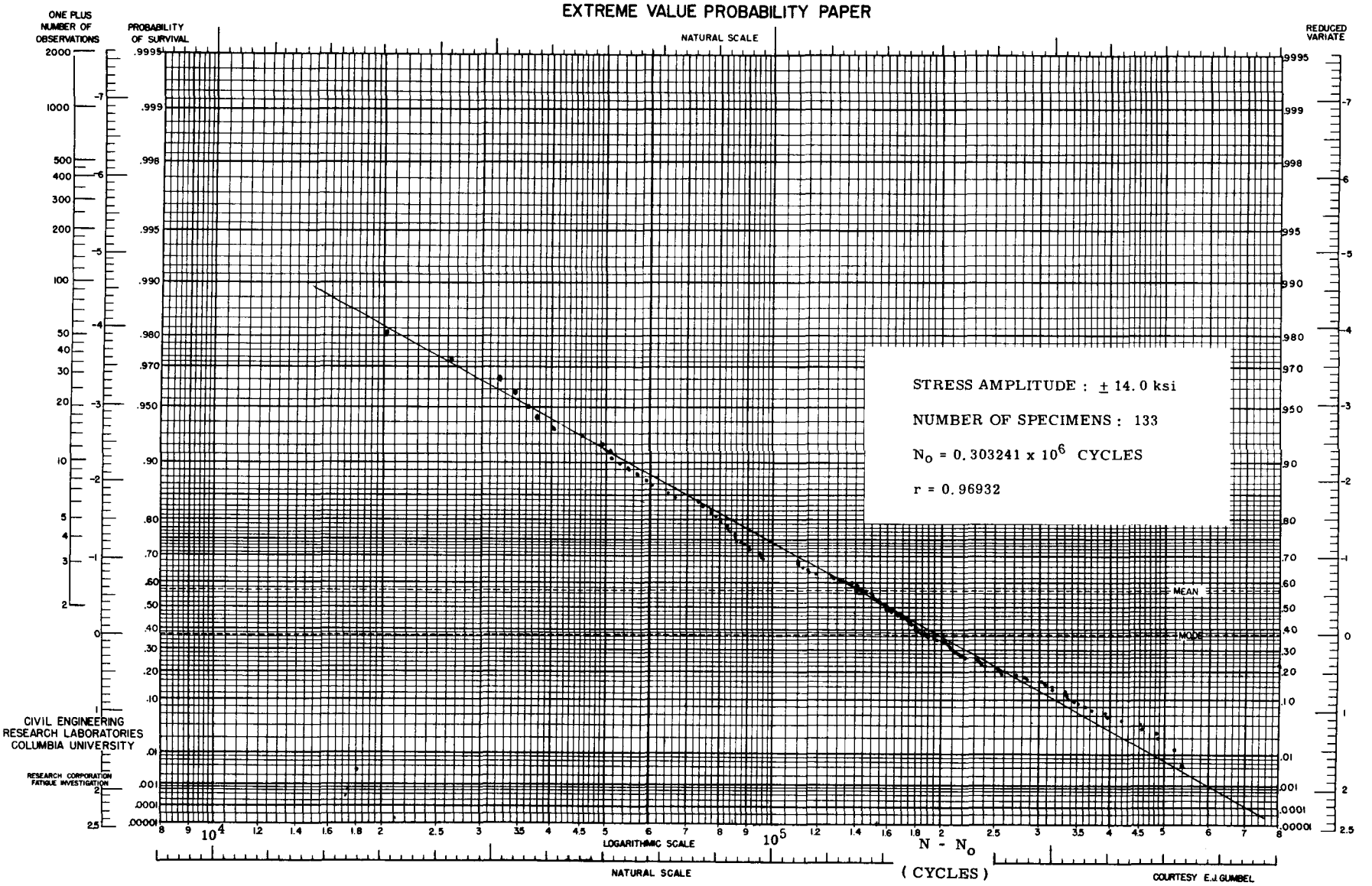

FIG. 10 (c) WEIBULL PROBABILITY PLOT, SINGLE DISTRIBUTION. PARAMETERS CALCULATED BY THE CLASSICAL MOMENT METHOD.

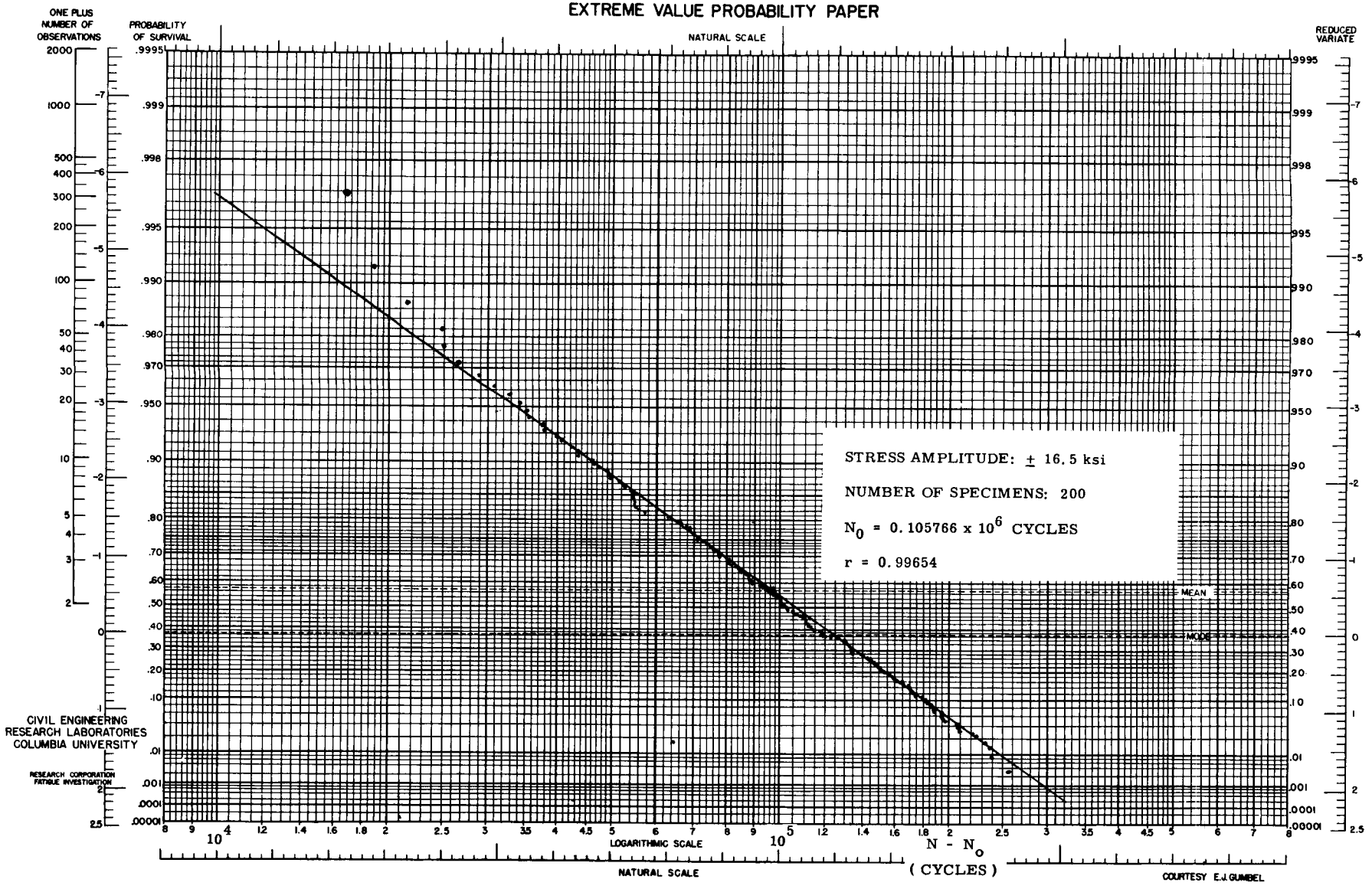

FIG. 10 (d) WEIBULL PROBABILITY PLOT, SINGLE DISTRIBUTION. PARAMETERS CALCULATED BY THE CLASSICAL MOMENT METHOD.

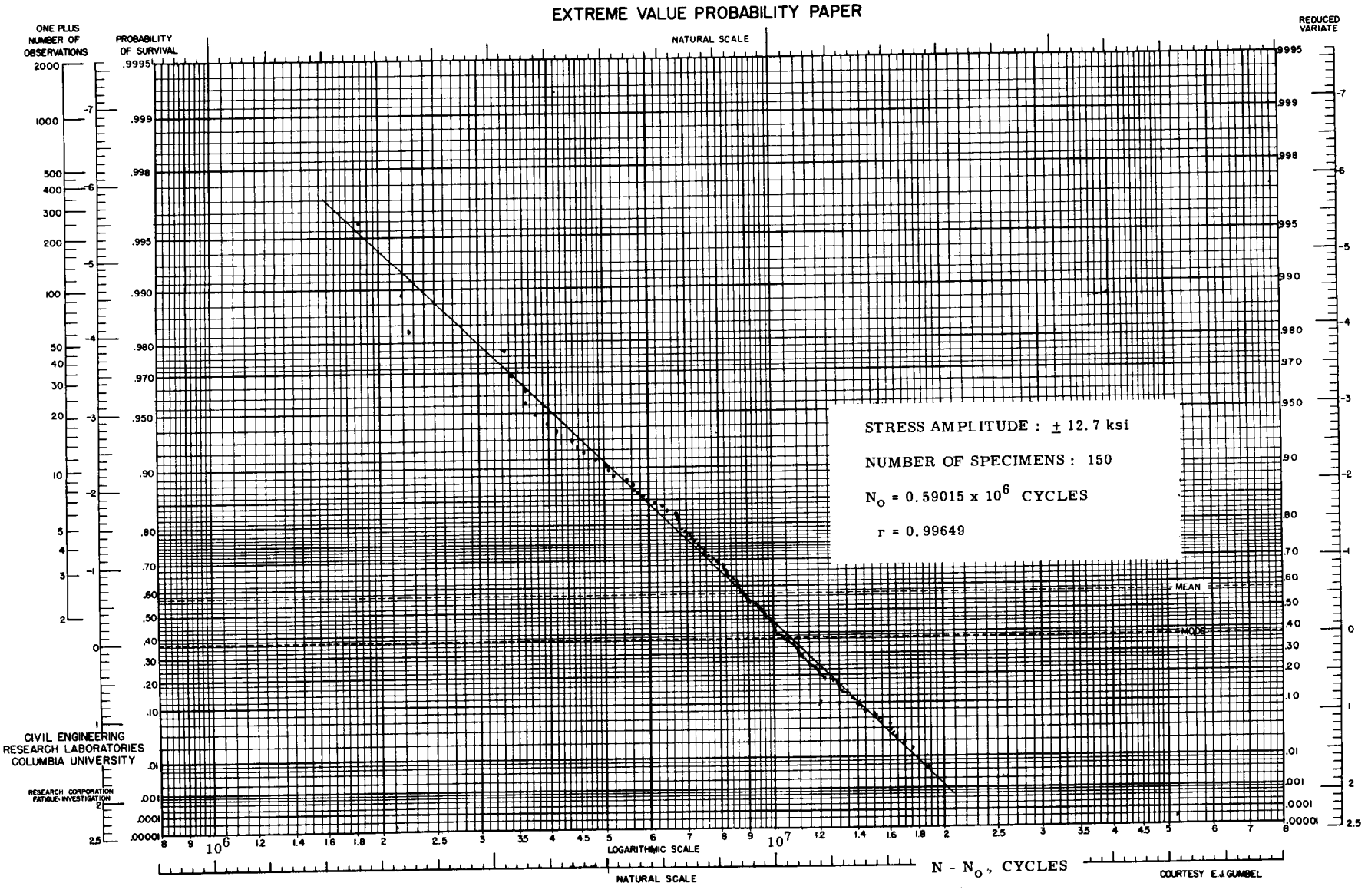

FIG. 11 (a) WEIBULL PROBABILITY PLOT, SINGLE DISTRIBUTION. PARAMETERS CALCULATED BY THE UPPER VERTICAL MOMENT METHOD.

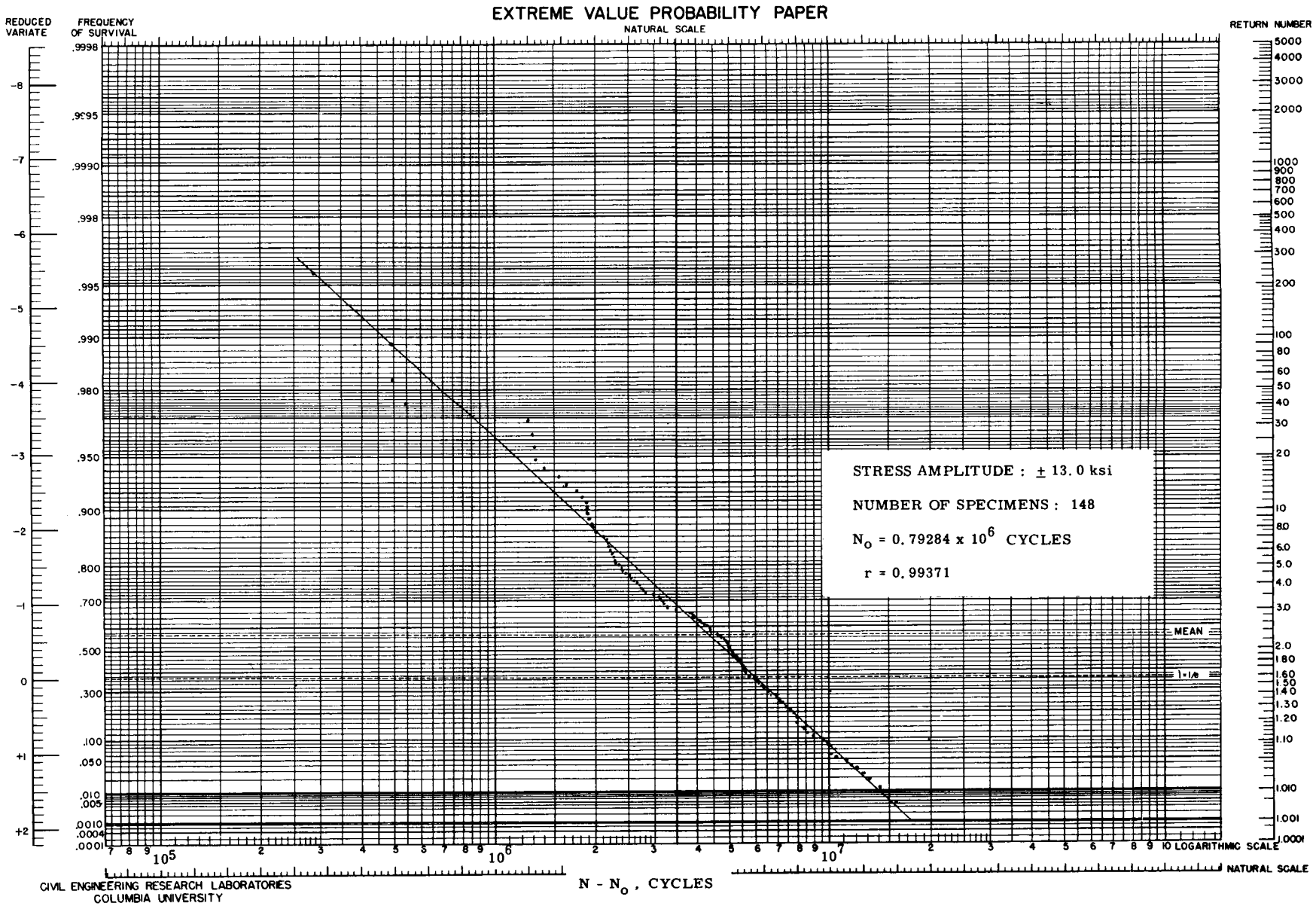

FIG. 11 (b) WEIBULL PROBABILITY PLOT, SINGLE DISTRIBUTION. PARAMETERS CALCULATED BY THE UPPER VERTICAL MOMENT METHOD.

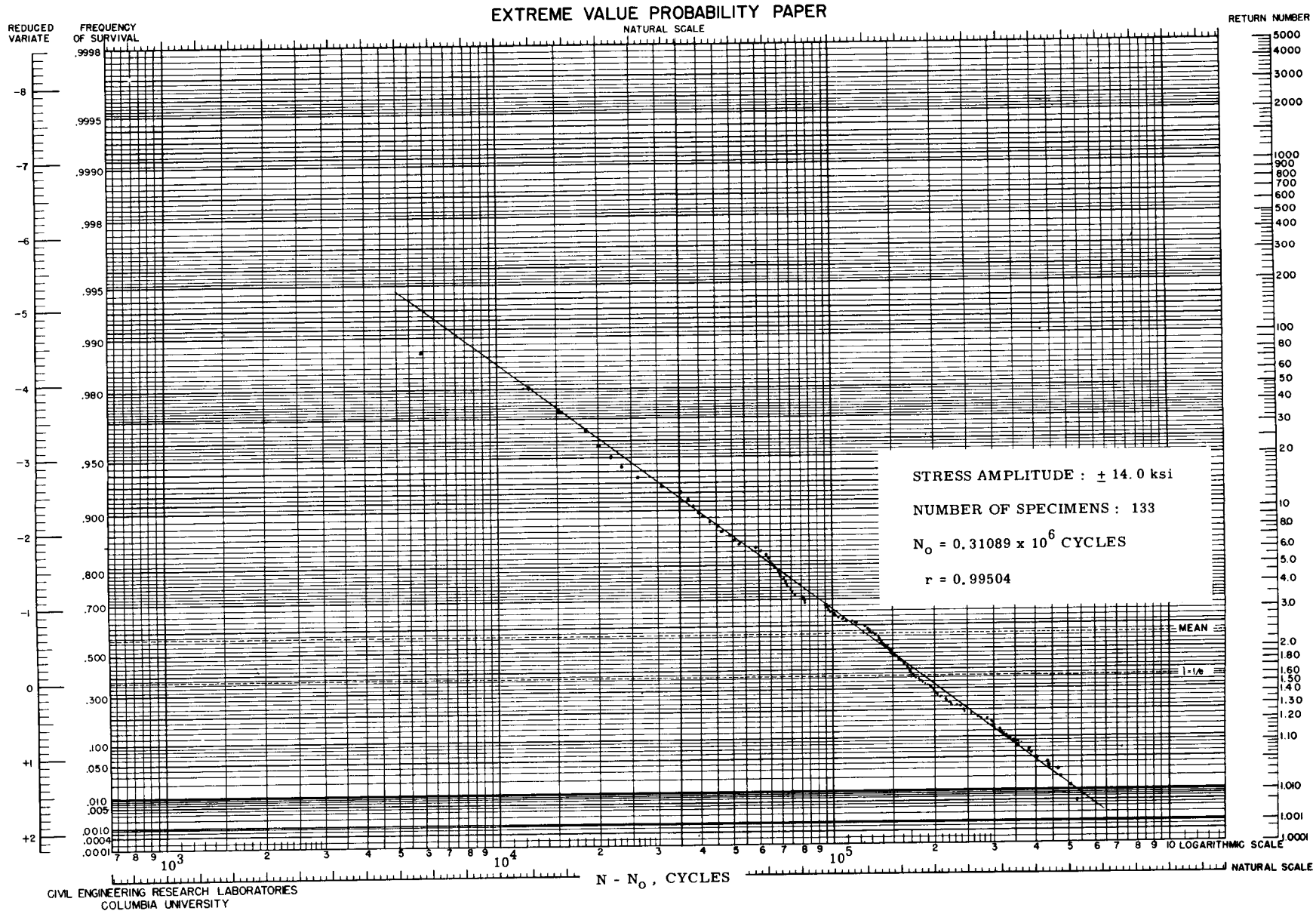

FIG. 11 (c) WEIBULL PROBABILITY PLOT, SINGLE DISTRIBUTION. PARAMETERS CALCULATED BY THE UPPER VERTICAL MOMENT METHOD.

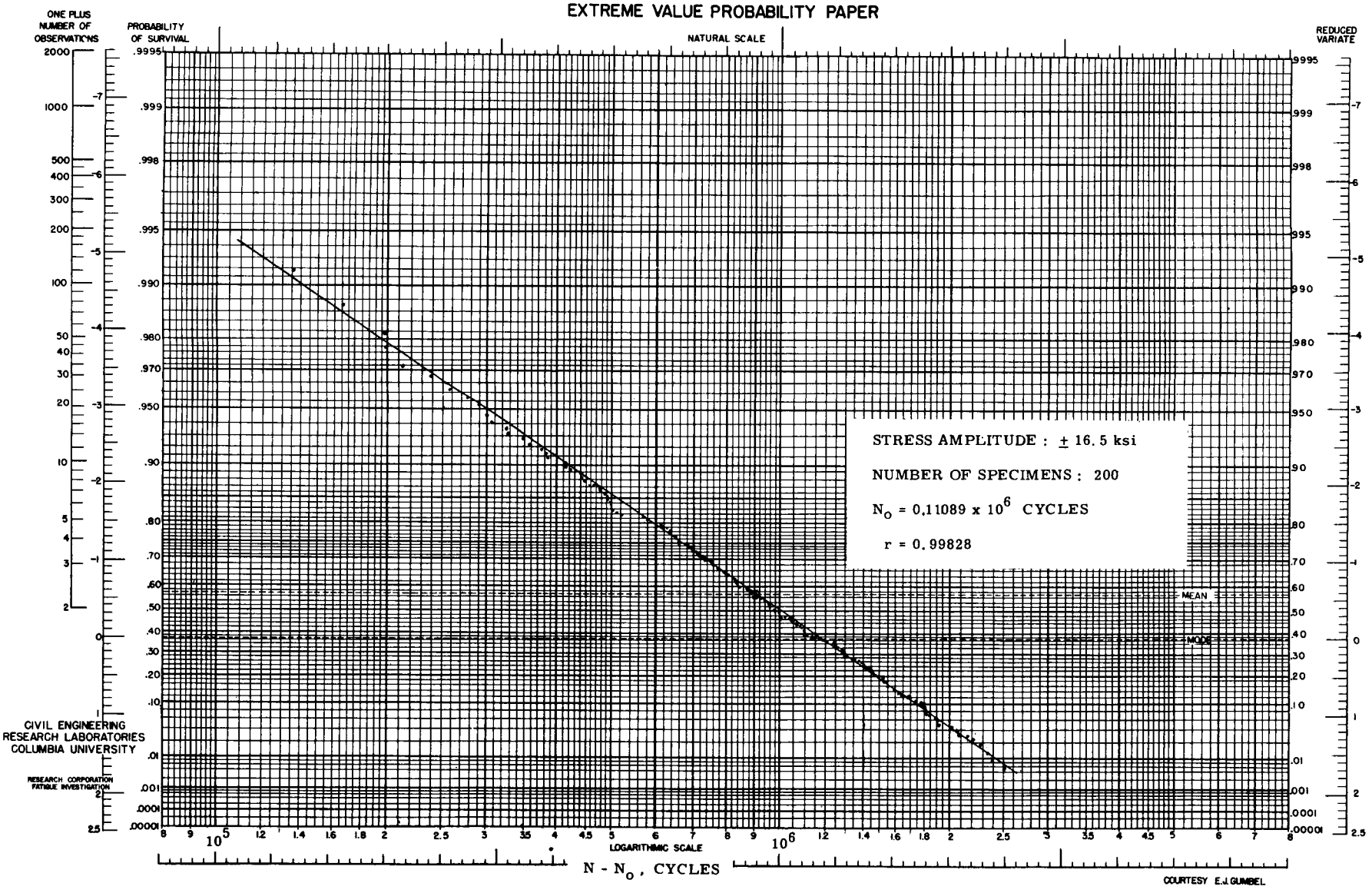

FIG. 11 (d) WEIBULL PROBABILITY PLOT, SINGLE DISTRIBUTION. PARAMETERS CALCULATED BY THE UPPER VERTICAL MOMENT METHOD.

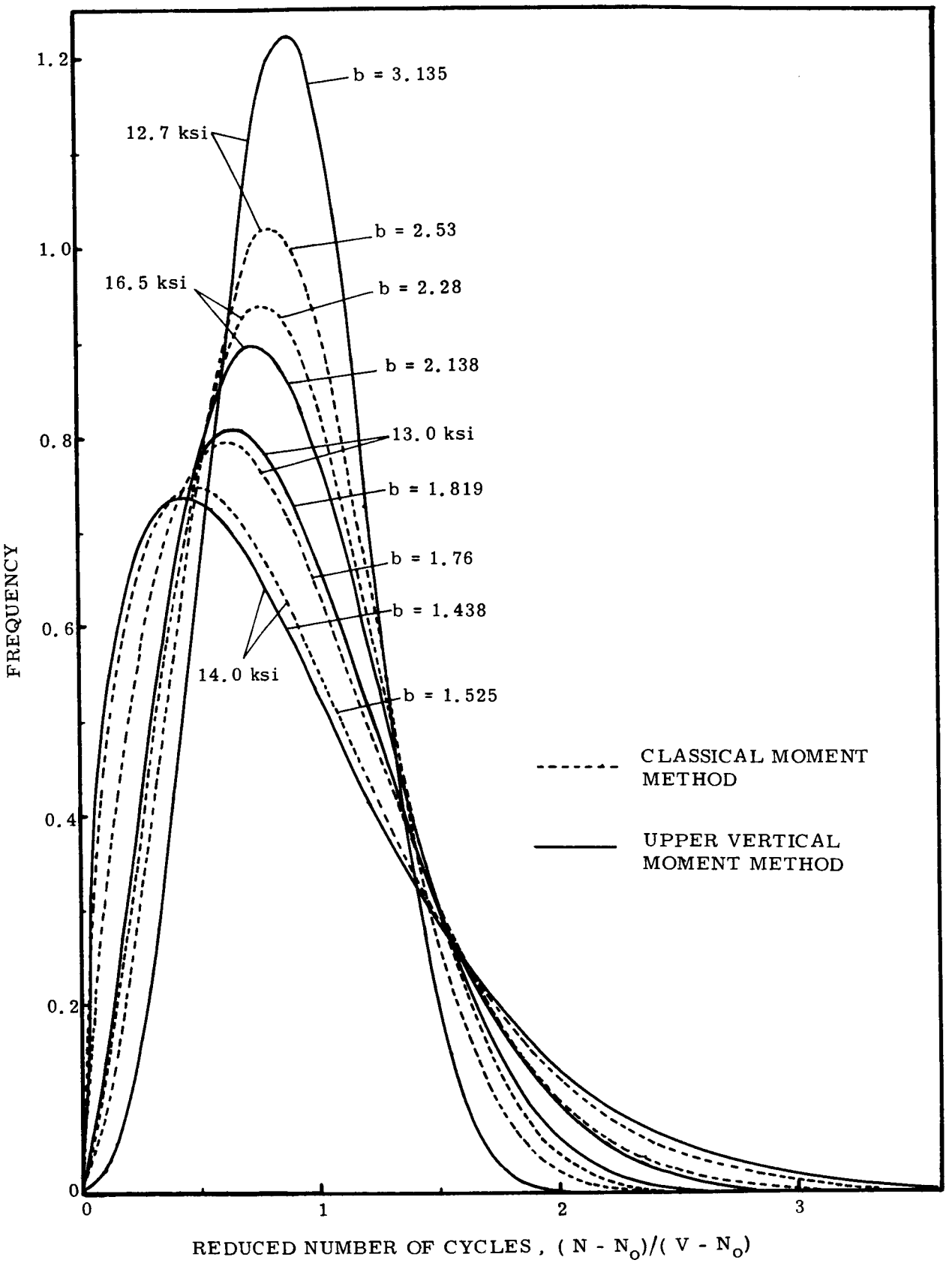

FIGURE 12 WEIBULL FREQUENCY DISTRIBUTION CURVES

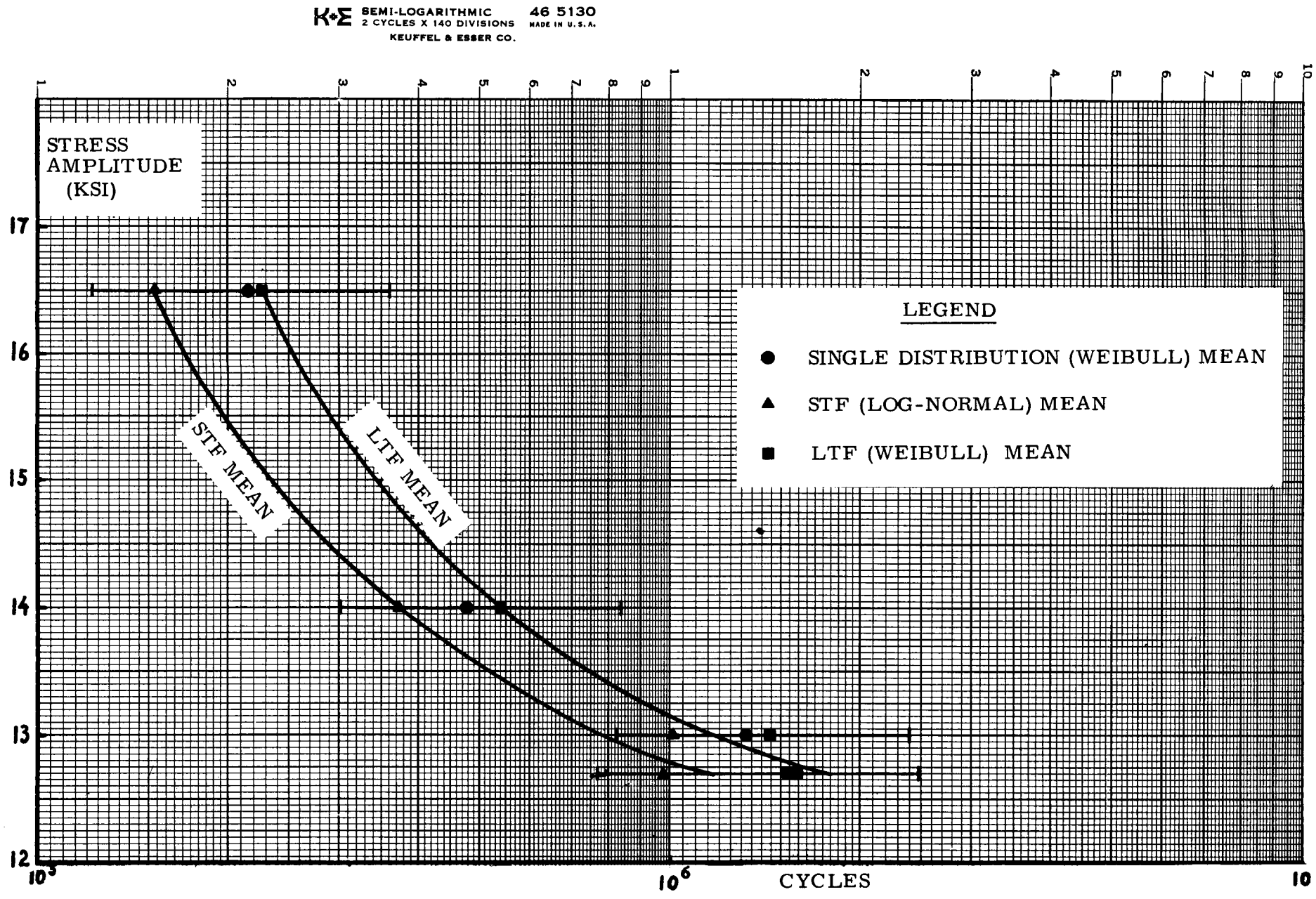

FIG. 13 (a) S - N CURVE WITH SCATTER RANGES AND DISTRIBUTION MEANS

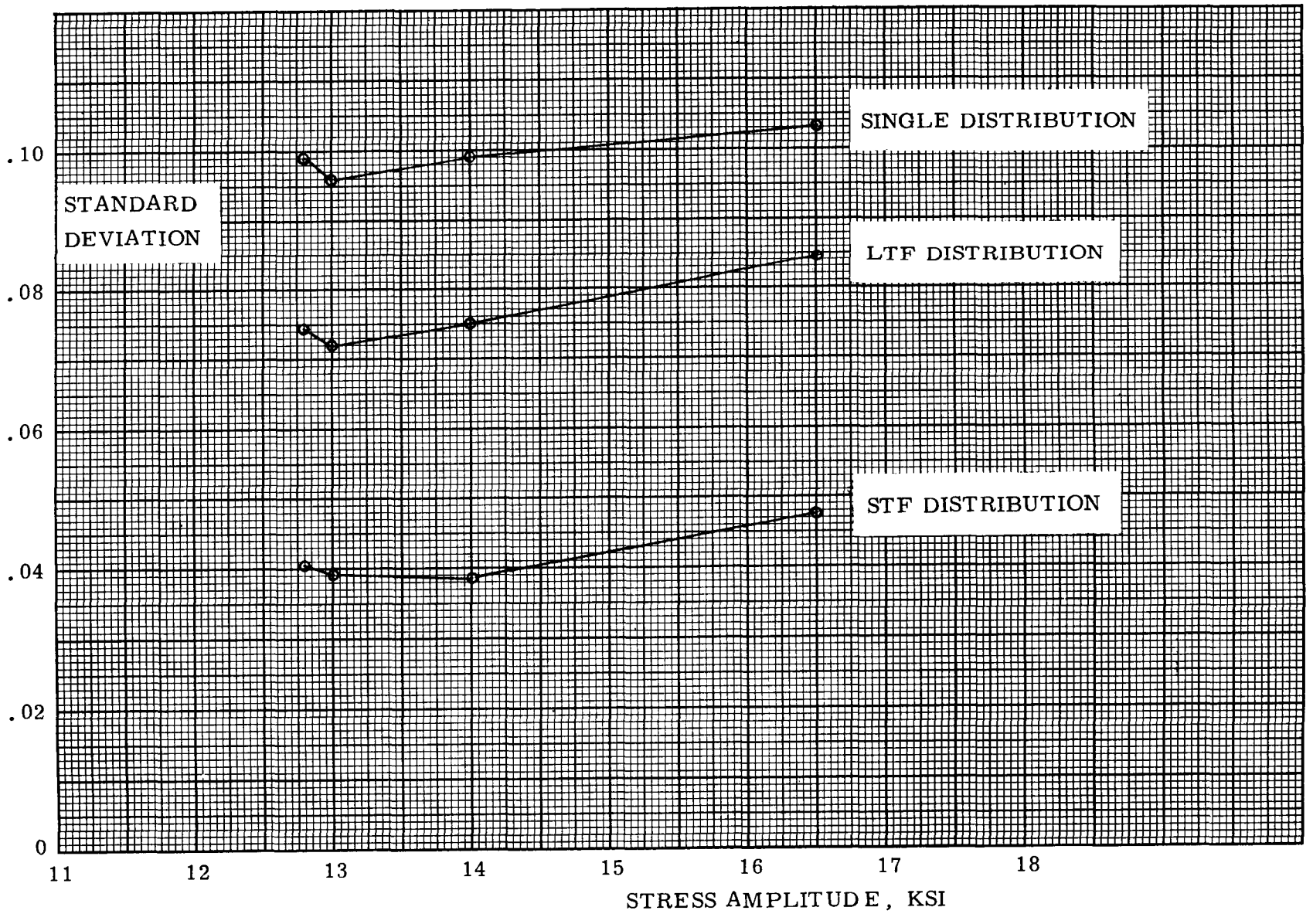

FIG. 13 (b) VARIATION IN STANDARD DEVIATION WITH STRESS AMPLITUDE

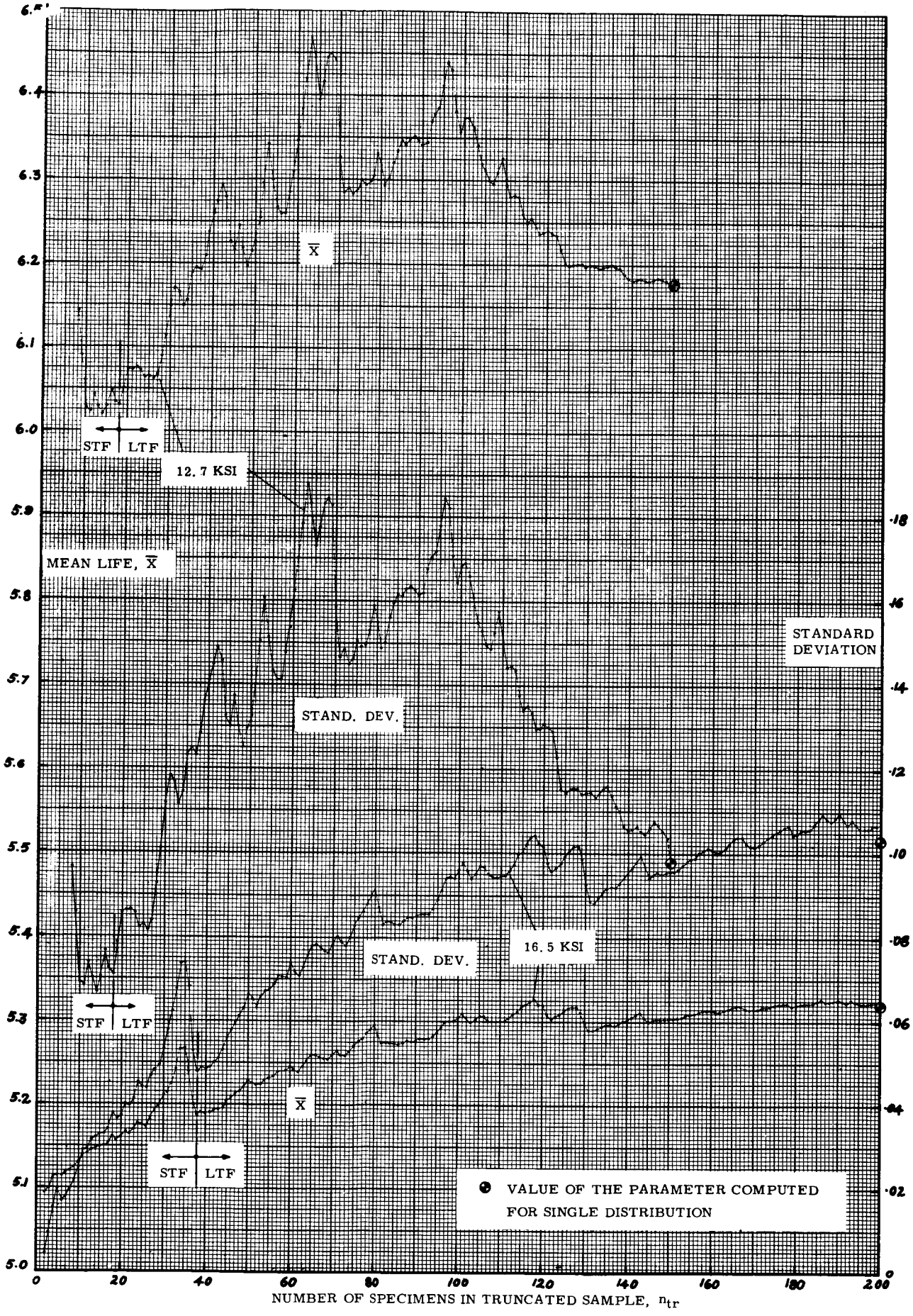

FIG. 14 (a) PARAMETERS OF THE TRUNCATED LOG-NORMAL DISTRIBUTION. HIGH-ENDURANCE PART EXCLUDED. 12.7 KSI AND 16.5 KSI STRESS LEVELS

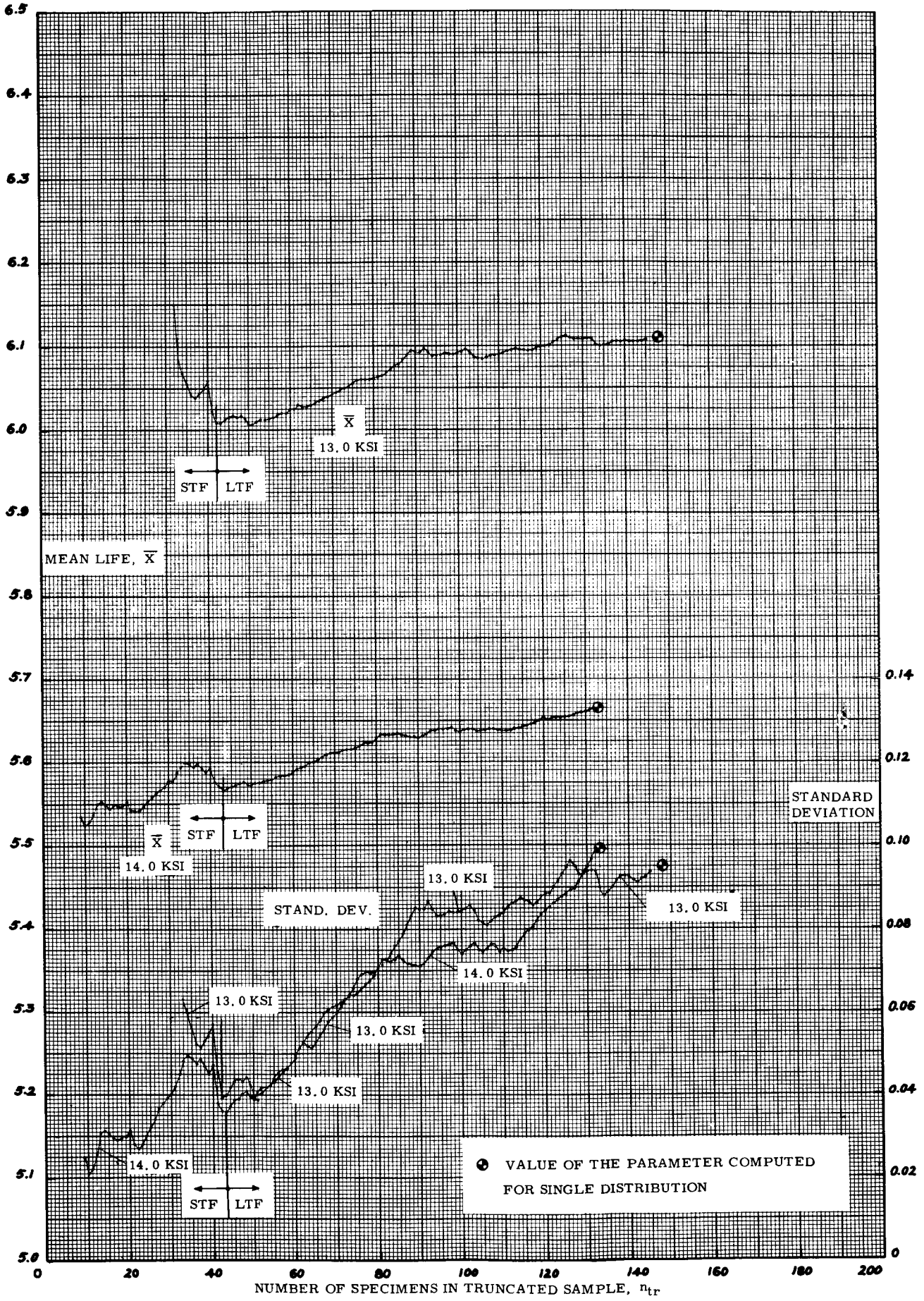

FIG. 14 (b) PARAMETERS OF THE TRUNCATED LOG-NORMAL DISTRIBUTION. HIGH-ENDURANCE PART EXCLUDED. 13.0 KSI AND 14.0 KSI STRESS LEVELS

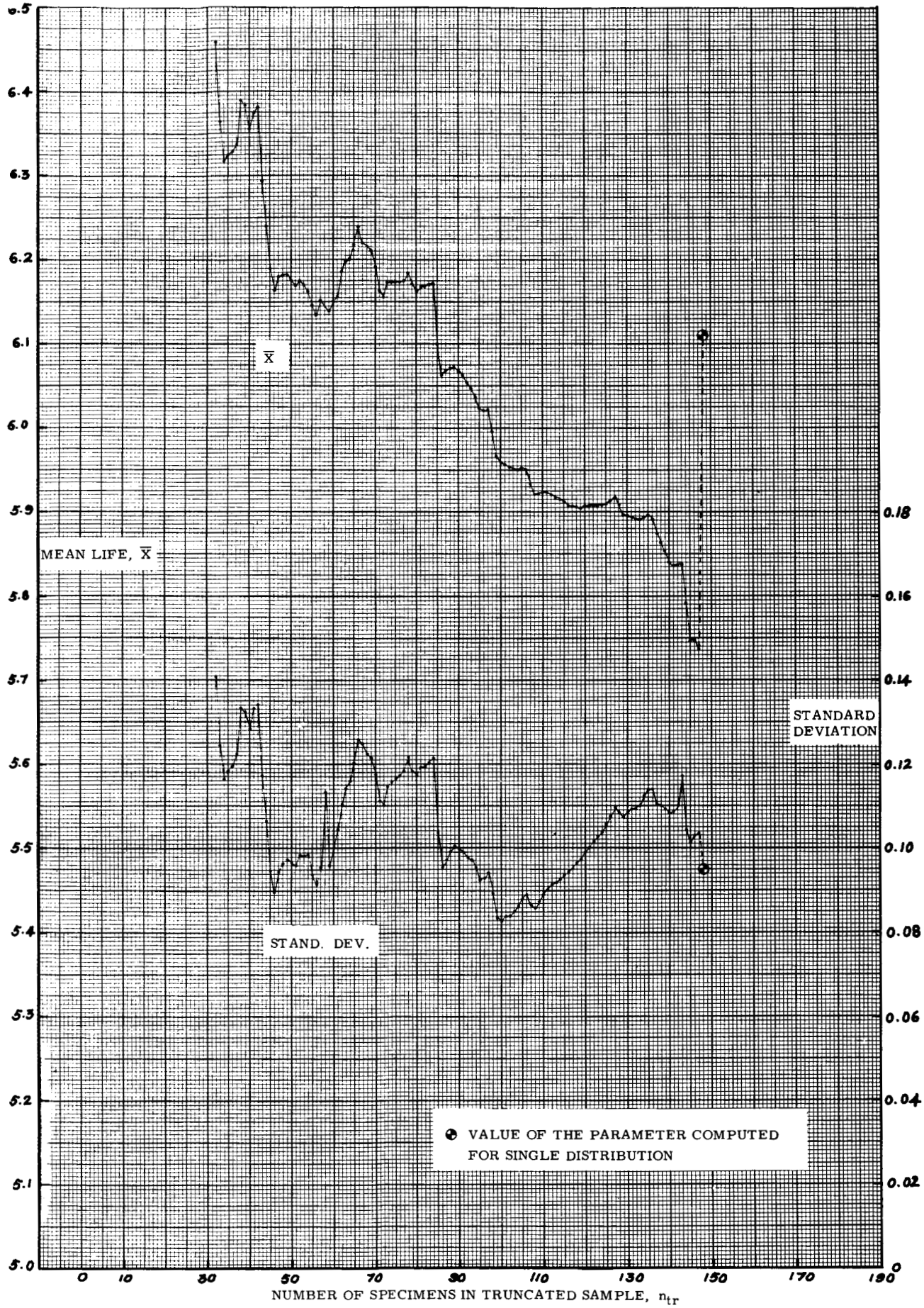

FIG. 15 (a) PARAMETERS OF THE TRUNCATED LOG-NORMAL DISTRIBUTION.
LOW-ENDURANCE PART EXCLUDED.
13.0 KSI STRESS LEVEL

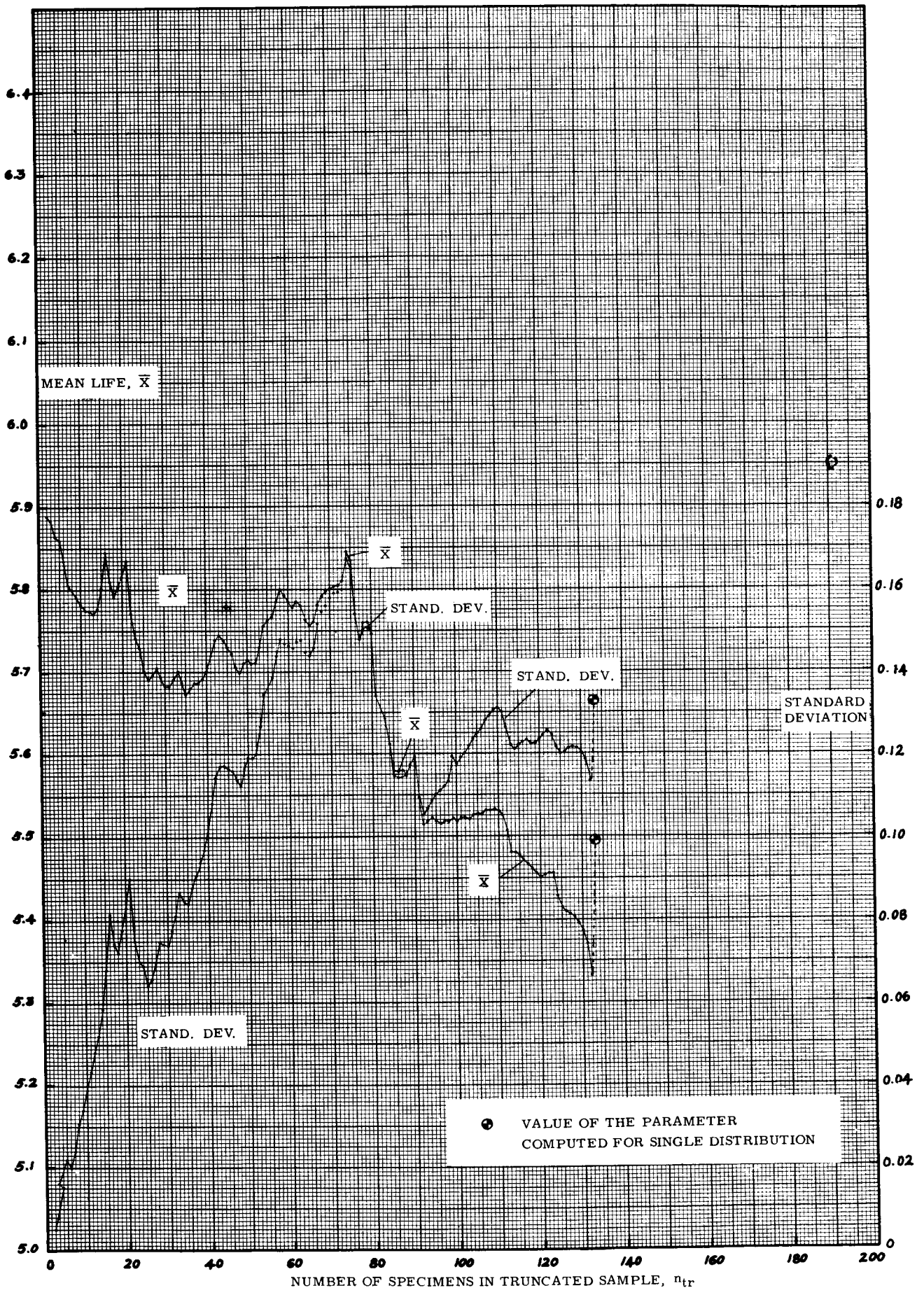

FIG. 15 (b) PARAMETERS OF THE TRUNCATED LOG-NORMAL DISTRIBUTION.
LOW-ENDURANCE PART EXCLUDED.
14.0 KSI STRESS LEVEL

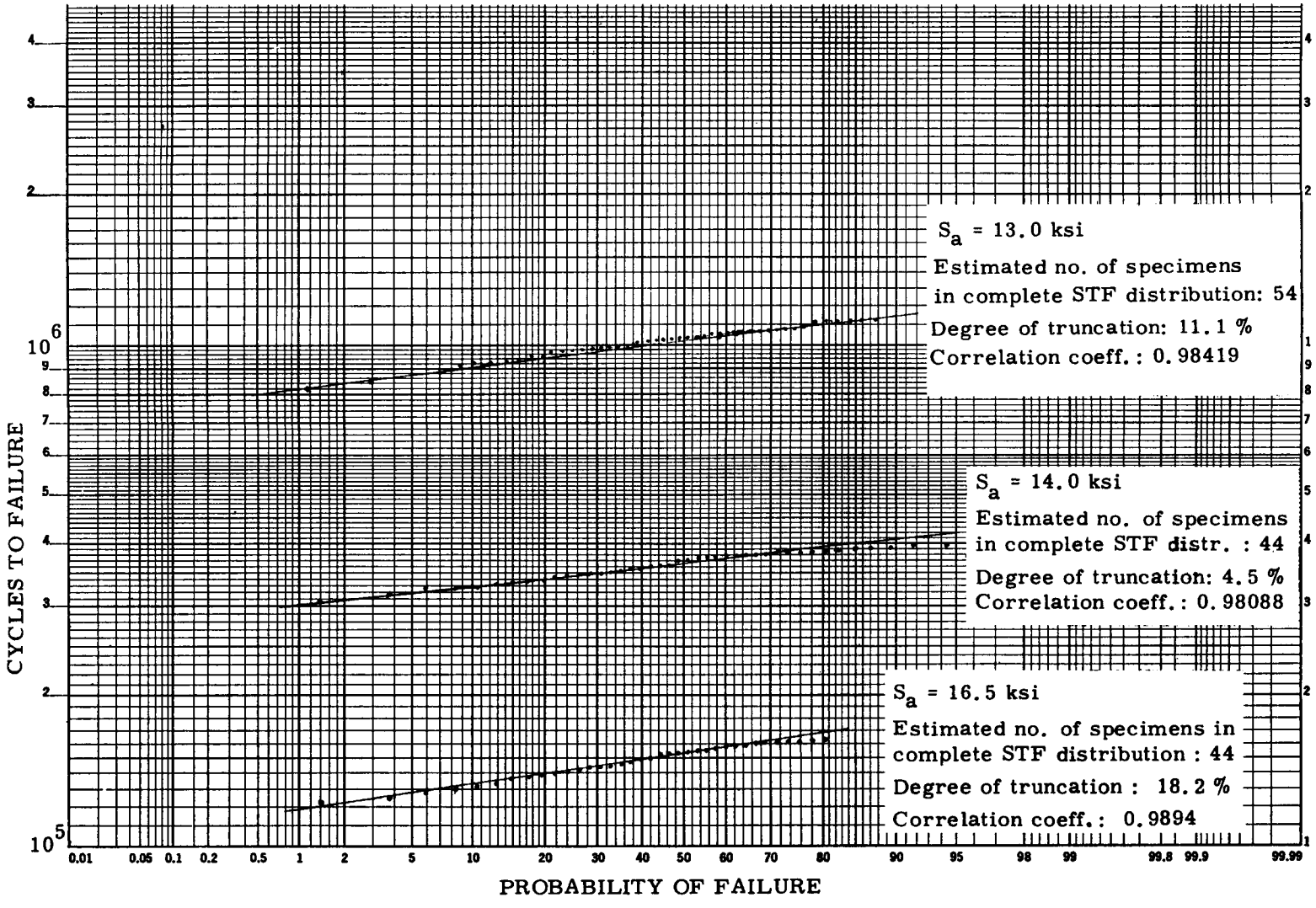

FIG. 16 TWO-DISTRIBUTION PRESENTATION OF RESULTS. LOG-NORMAL PROBABILITY PLOTS OF STF COMPONENT DISTRIBUTION.

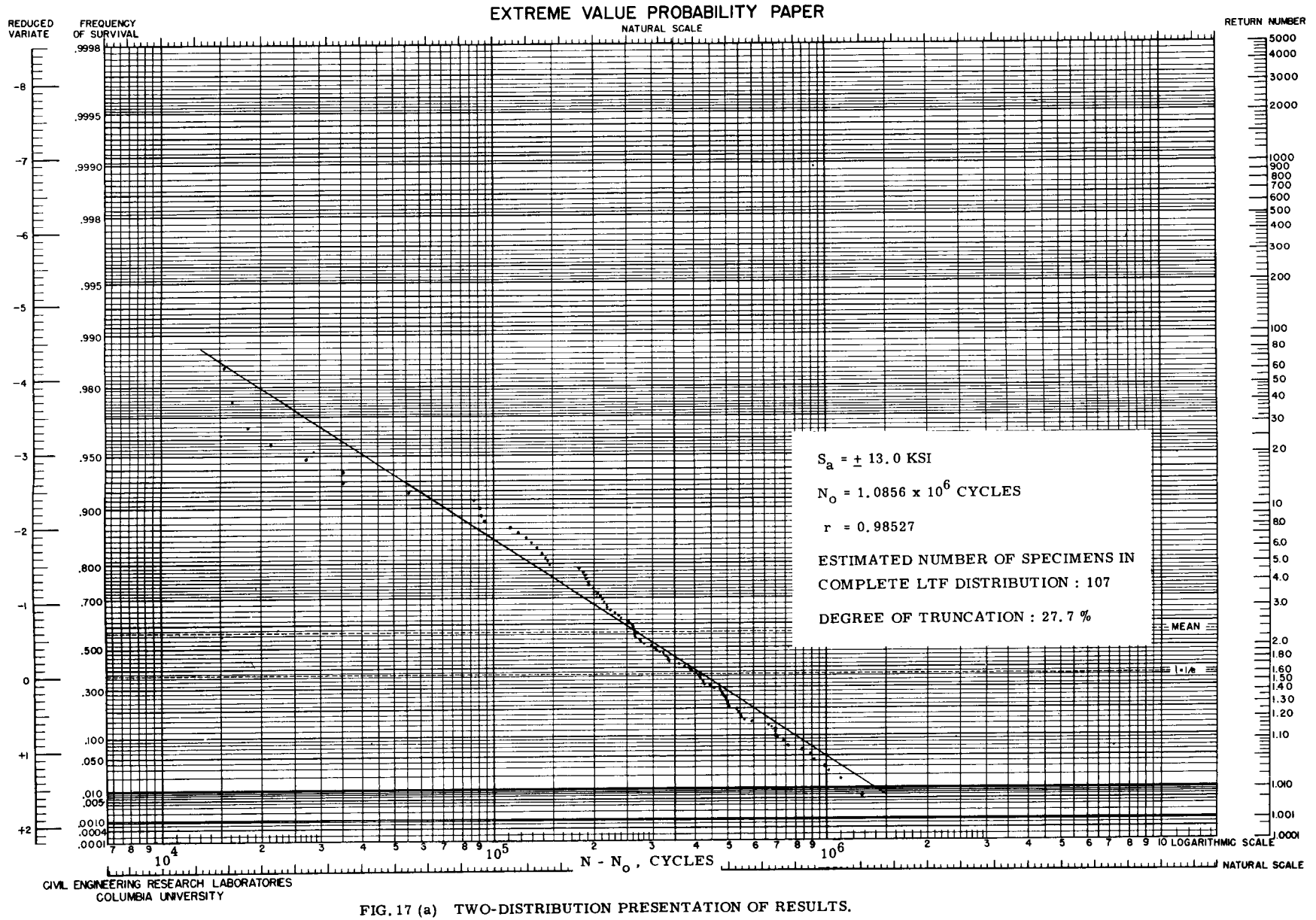

FIG. 17 (a) TWO-DISTRIBUTION PRESENTATION OF RESULTS.
WEIBULL PROBABILITY PLOT OF HIGH-ENDURANCE (LTF) COMPONENT.
PARAMETERS CALCULATED BY THE UPPER VERTICAL MOMENT METHOD.

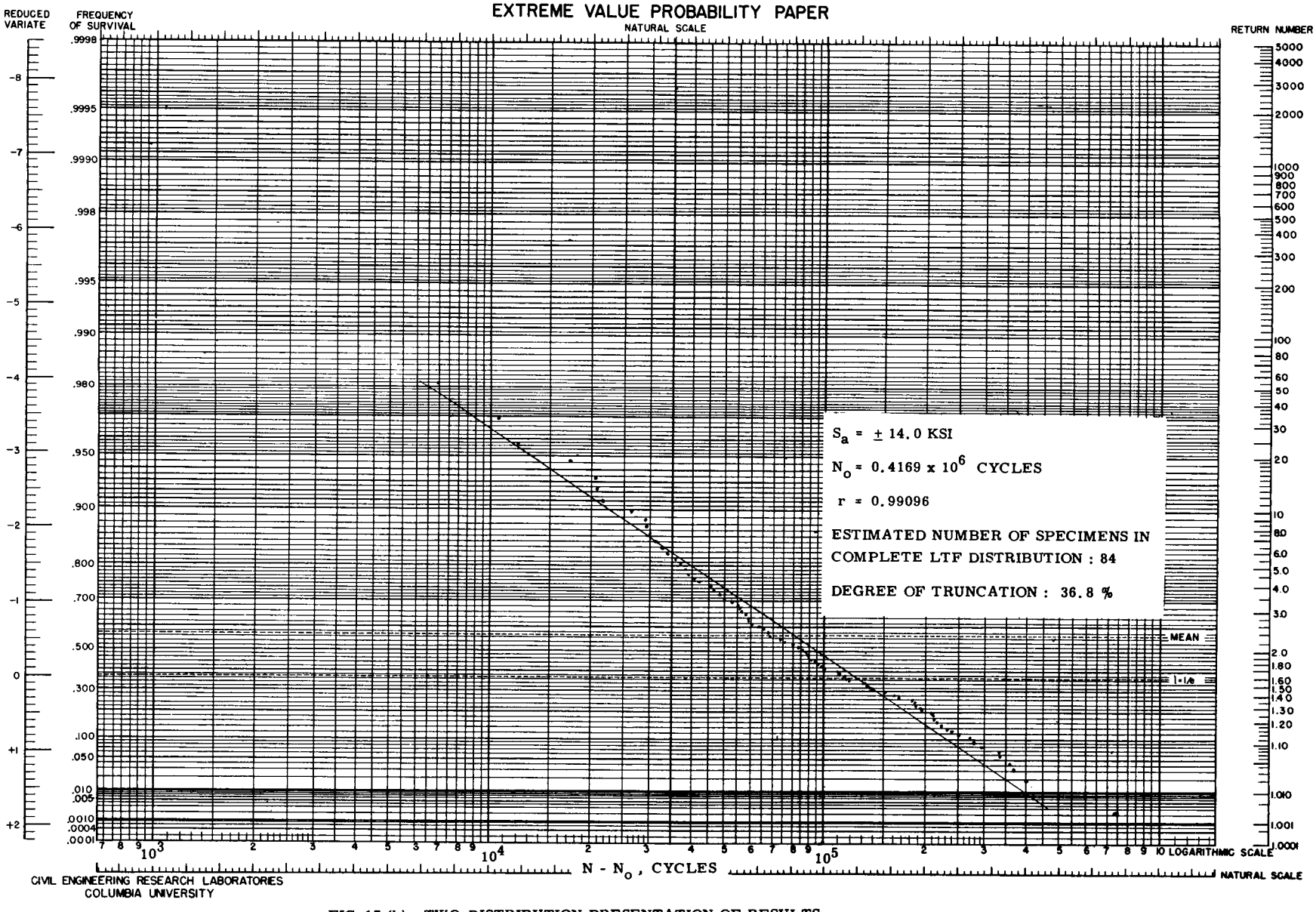

FIG. 17 (b) TWO-DISTRIBUTION PRESENTATION OF RESULTS.
WEIBULL PROBABILITY PLOT OF HIGH-ENDURANCE (LTF) COMPONENT.
PARAMETERS CALCULATED BY THE UPPER VERTICAL MOMENT METHOD.

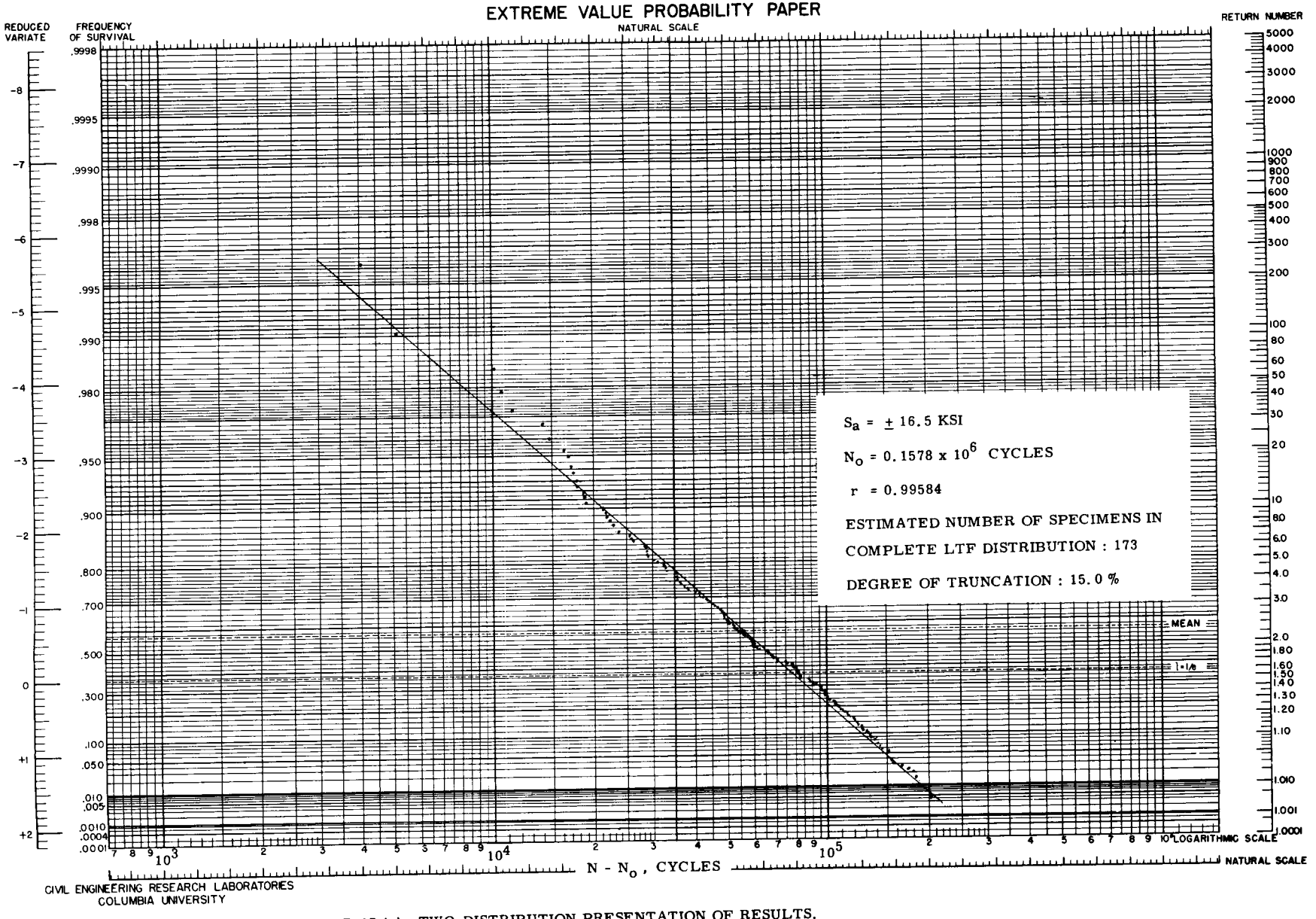

FIG. 17 (c) TWO-DISTRIBUTION PRESENTATION OF RESULTS.
WEIBULL PROBABILITY PLOT OF HIGH-ENDURANCE (LTF) COMPONENT.
PARAMETERS CALCULATED BY THE UPPER VERTICAL MOMENT METHOD.

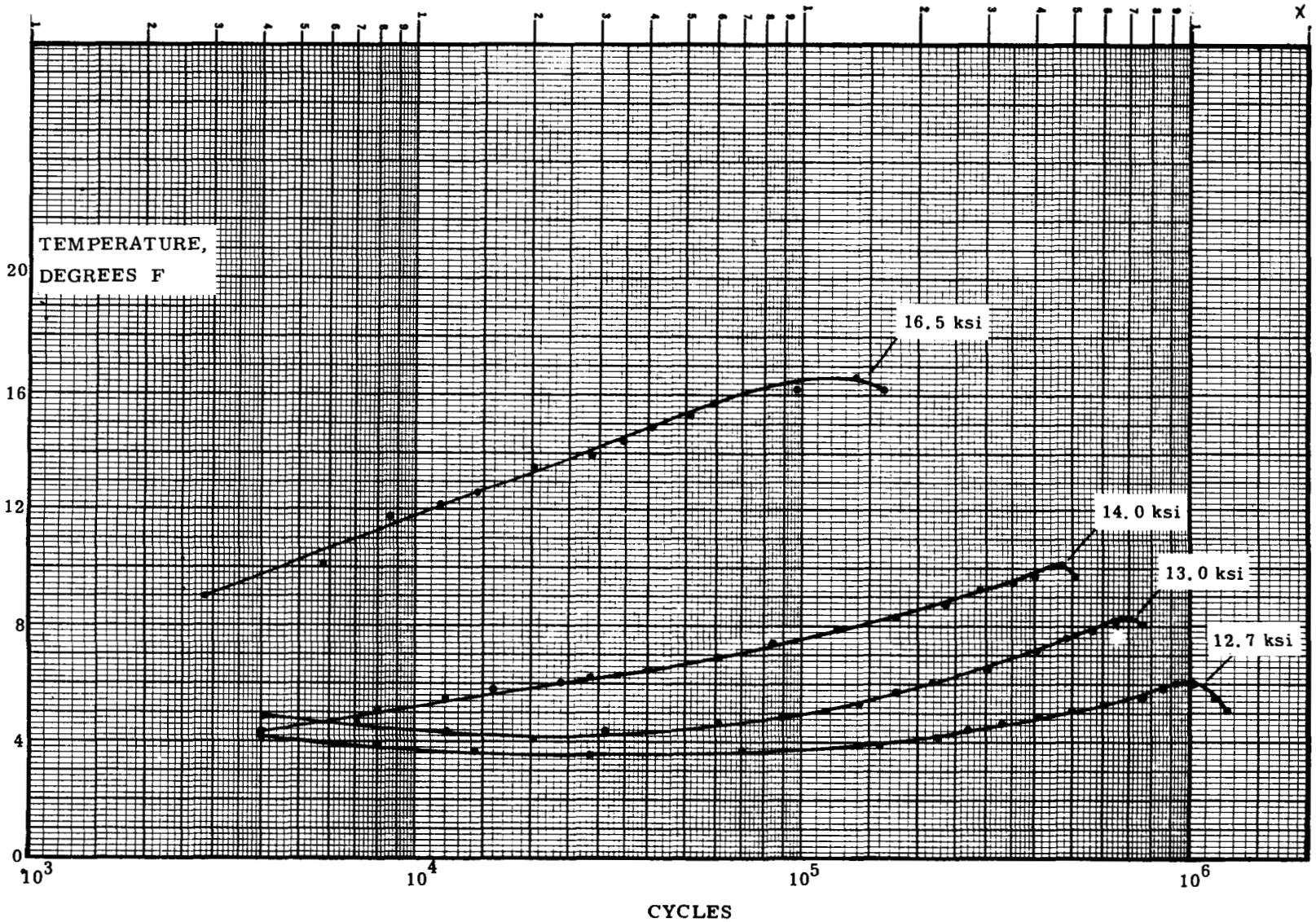

FIG. 18 TEMPERATURE INCREASE (ABOVE ROOM TEMPERATURE) IN THE FATIGUE SPECIMENS WITH NUMBER OF CYCLES

TOP →